9 Accidental and Non-accidental Articular Injuries in the Skeletally Immature Patient

9.1 Introduction

The notion that children are not small adults is proverbial in medicine. This is also valid for osteoarticular trauma, as the immature musculoskeletal system responds to traumatic injuries differently from the adult organism. Lesions due to acute high-energy trauma, which are discussed in this chapter, differ from those caused by overuse/anomalous stress, such as the sports-related injuries studied in Chap. 10. Special emphasis will be put on articular injuries, although some extraarticular lesions typical of the pediatric age group are also described. In addition to accidental traumatic injuries, this chapter will also cover non-accidental trauma, given the importance of imaging as an objective evidence of child abuse. A concise approach will be used in the following topics, highlighting the imaging appearance of the most frequent lesions. Pediatric trauma is an extensive and complex issue and an in-depth study of it is beyond the scope of this brief review.

9.2 Peculiar Aspects of the Fractures of the Immature Skeleton

The most important difference between the immature skeleton and the adult organism is the presence of the physis, a specialized region located in the transition between the metaphysis and the epiphysis (see Chap. 2), which is most vulnerable in the provisional calcification zone. Because of its high collagen content, the immature bone is weaker than the adjacent ligaments and tendons, and traumatic lesions that would lead only to ligament injuries in adults may cause fractures in children. Nonetheless, the bones of children are more elastic than the undeformable bones of adults, so that pediatric fractures are less prone to propagation/comminution. As the periosteum is thicker, more active, and more resistant in children than in adults, there is speedy callus formation and prompt healing of fractures in the former.

Radiographs are indispensable in the initial assessment of a suspected fracture, and at least two orthogonal views are mandatory in order to describe the affected bone segments, the extent and the orientation of the fracture line, and the occasional presence of comminution, diastasis, angulation, or displacement (Figs. 9.1 and 9.2). The joints above and below the region of interest must be included in the radiographs, aiming to demonstrate physeal/intra-articular compromise or concomitant dislocation, which often go unnoticed. Indirect radiographic signs of fracture include displacement of periarticular fat planes (an indicator of joint effusion), irregularity of bone surfaces, abnormal alignment between the epiphysis, and the metaphysis and focal physeal widening (Fig. 9.3).

Computed tomography (CT), magnetic resonance imaging (MRI), and ultrasonography (US) are usually electively performed, as a second line of investigation. CT is very useful in diagnosing and staging fractures, especially in patients with inconclusive radiographs or in regions of complex anatomy, being also helpful in the assessment of late complications (Fig. 9.4). MRI is very suitable to evaluate soft-tissue structures and to evidence the presence of bone marrow edema pattern, a reliable marker of bone alterations that may herald “hidden” fractures (Figs. 9.5 and 9.6). Because of its appropriateness for the study of the non-ossified cartilage, MRI is also valuable in the evaluation of physeal fractures and in the assessment of joint dislocations in small children (Fig. 9.7). Bone scintigraphy has high sensitivity in the detection of fractures, being able to evaluate the whole skeleton in a single study; the latter feature is especially useful in the screening of fractures, such as those found in polytraumatized or physically abused children. However, because of its low specificity and limited spatial resolution, most areas of abnormal uptake demand additional investigation in order to determine their real nature. US is more adequate for the assessment of soft-tissue abnormalities associated with fractures, such as joint effusion, periosteal detachment, and periarticular fluid collections. In addition, fractures of the non-ossified portions of the ossification centers (which are undetectable on radiographs) may be diagnosed with US (Fig. 9.8).

S.L. Viana et al., *Joint Imaging in Childhood and Adolescence*,
DOI 10.1007/978-3-642-35876-0_9, © Springer-Verlag Berlin Heidelberg 2013

Fig. 9.1 Anteroposterior view (*left*) and lateral view (*right*) of the right ankle of a child with triplanar fracture. The *first image* shows a vertical fracture affecting the lateral portion of the distal epiphysis of the tibia and lateral physeal widening, which could be taken as a Salter-Harris fracture type III. Nonetheless, there is a bone fragment projected posterior and lateral to the distal metaphysis of the tibia, better seen in the lateral view, which demonstrates a coronal fracture of the metaphysis. Complex fractures like this one require CT for proper evaluation

Fig. 9.2 Lateral view of the left ankle demonstrating a type II fracture of the distal tibia with anterior displacement of the epiphysis and of the metaphyseal fragment. Marked osteoporosis is also present

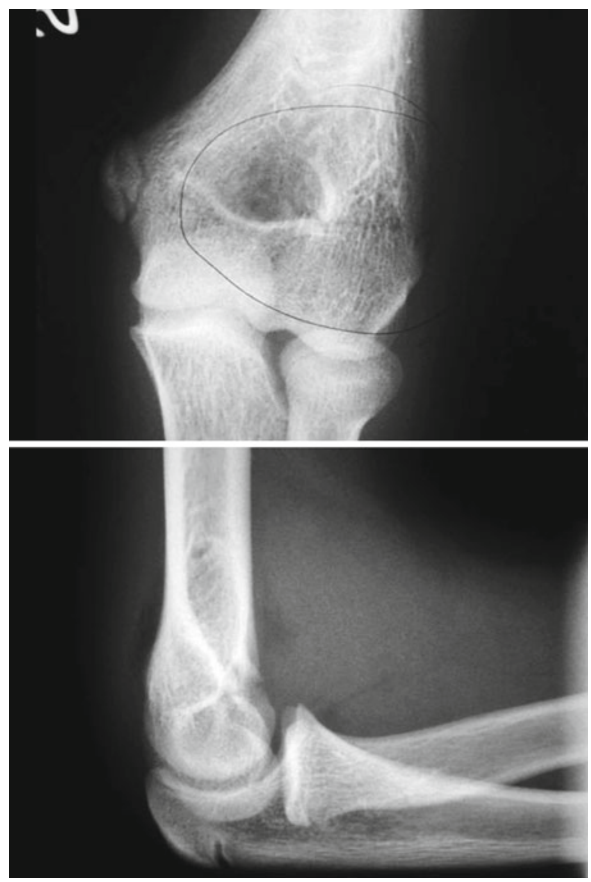

Fig. 9.3 Radiographs of the left elbow of a child with supracondylar fracture of the humerus. Although the fracture line is quite subtle in the anteroposterior view, additional markers seen on the lateral view include displacement of the anterior and posterior fat planes and absent intersection between the anterior humeral line and the central portion of the distal epiphysis

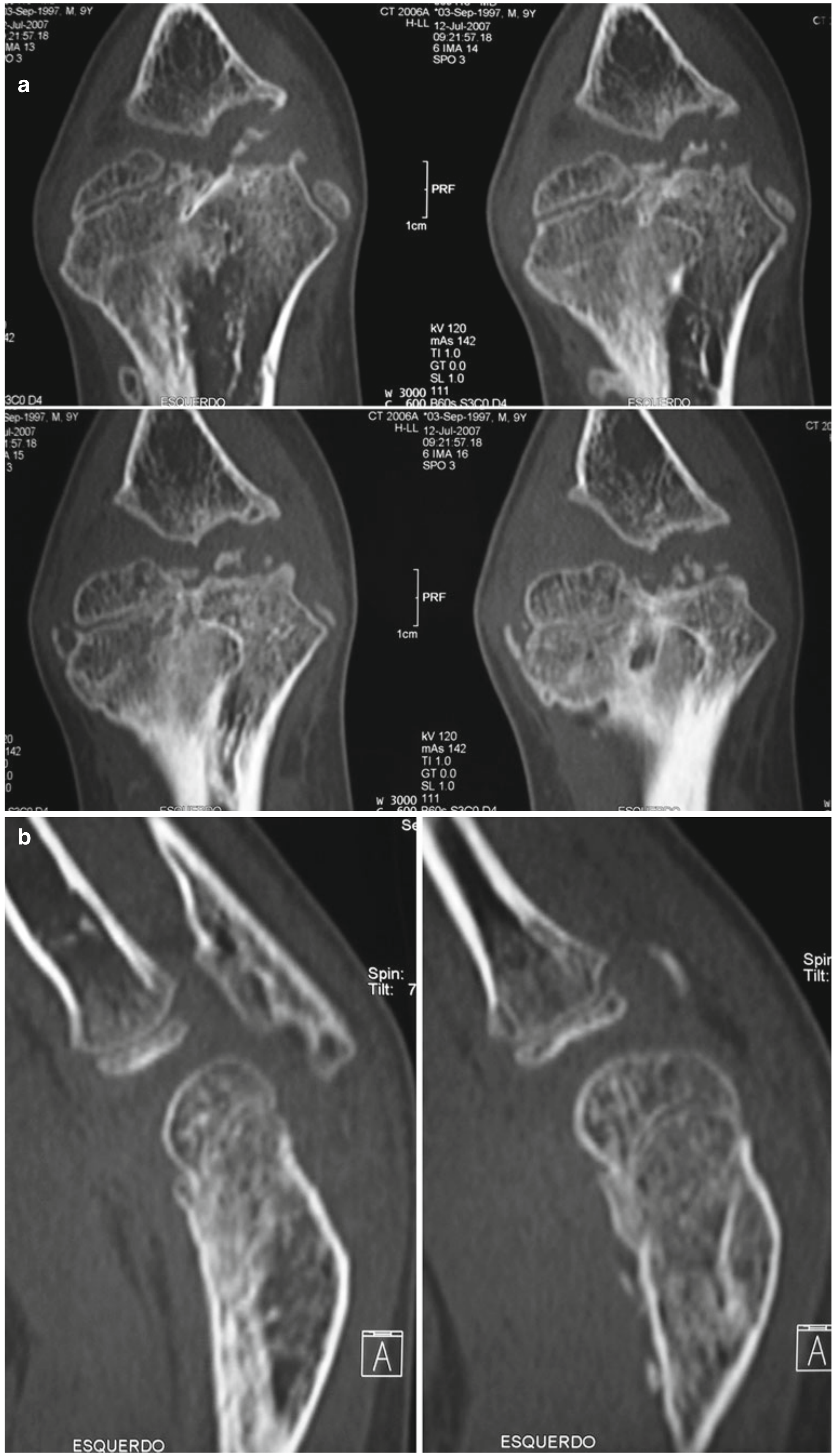

Fig. 9.4 Reformatted CT images in the coronal (**a**) and sagittal (**b**) planes of the distal humerus of a 9-year-old child show a healed transphyseal fracture (type IV) of the lateral condyle. There is a bony bridge between the humeral metaphysis and the anteromedial portion of the capitulum, more evident in (**b**). Premature osteoarthritis is also present

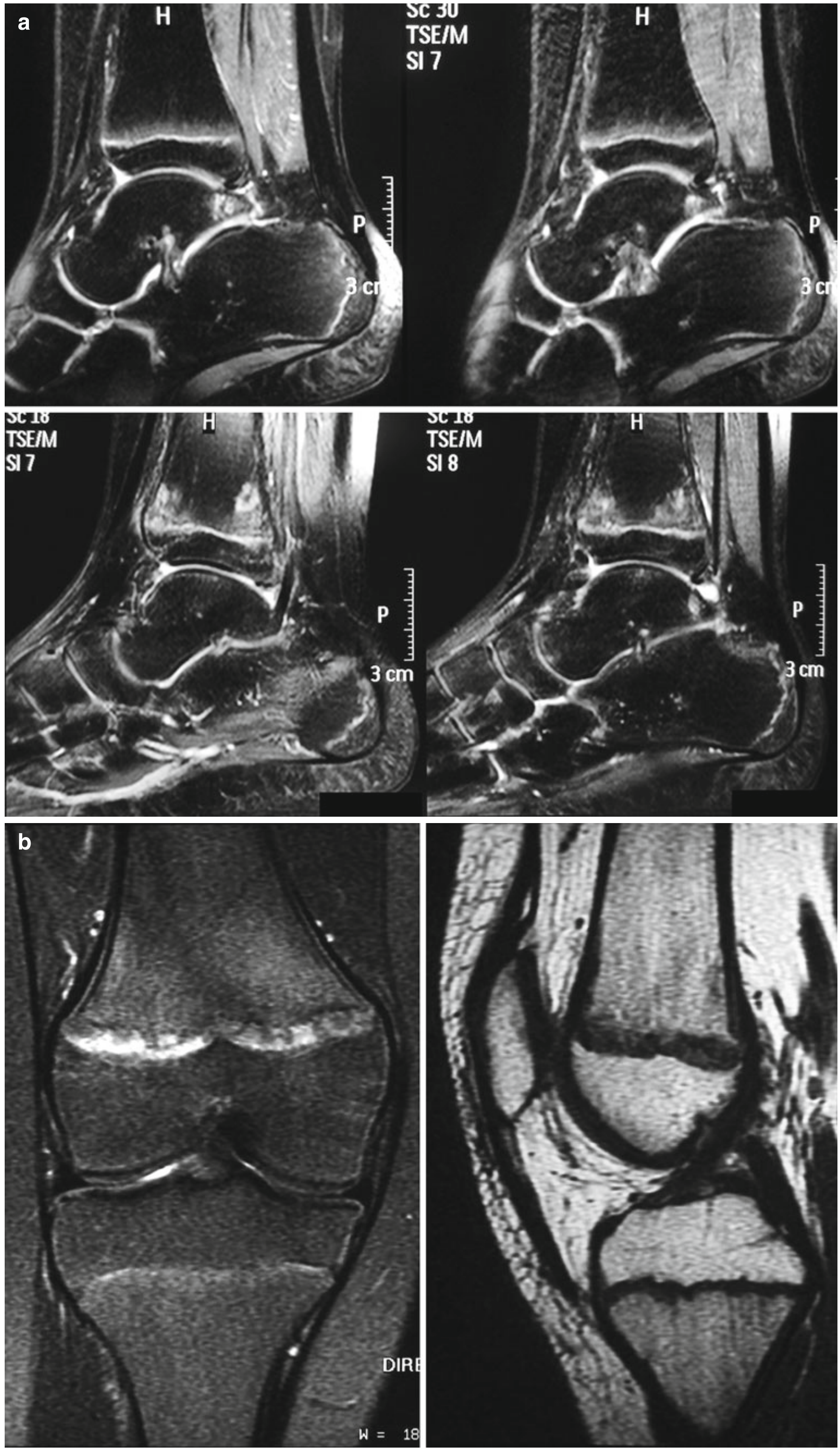

Fig. 9.5 In (**a**), sagittal fat sat T2-WI of the ankles (*right*, *upper row*; *left*, *lower row*) allows for clear demonstration of widening and increased signal intensity of the left tibial physis, as well as homolateral periphyseal edema. This acute, non-displaced Salter-Harris type I fracture would be difficult to detect with other imaging methods. Although similar findings are present in (**b**) (coronal fat sat PD-WI (*left*) and sagittal T1-WI (*right*) of the right knee of a 12-year-old child), bone marrow edema is less prominent and physeal widening is more evident, as this is a subacute lesion

Fig. 9.6 T1-WI (*left*) and fat sat T2-WI (*right*) of the left knee show subtle lateral displacement of the proximal epiphysis of the fibula, more evident in the coronal images (Salter-Harris lesion type I), with bone marrow edema pattern centered at the physis. There is also extensive edema in the adjacent muscles and a subperiosteal hematoma along the proximal metadiaphysis of the fibula

Fig. 9.7 In (**a**), radiographs of the left elbow demonstrate a fracture line involving the lateral condyle of the humerus, extending from the lateral cortex of the metaphysis to the physis, medial to the ossification center of the capitulum, which is already mineralized. Nonetheless, radiographs do not allow proper assessment of the extension of the fracture into the non-ossified portion of the epiphysis. Coronal T1-WI (**b**) is also limited to demonstrate the real extent of the fracture, which is clearly shown on fat sat PD-WI (**c**) (Salter-Harris fracture type IV). Joint effusion and marked edema of the periarticular soft tissues are also present

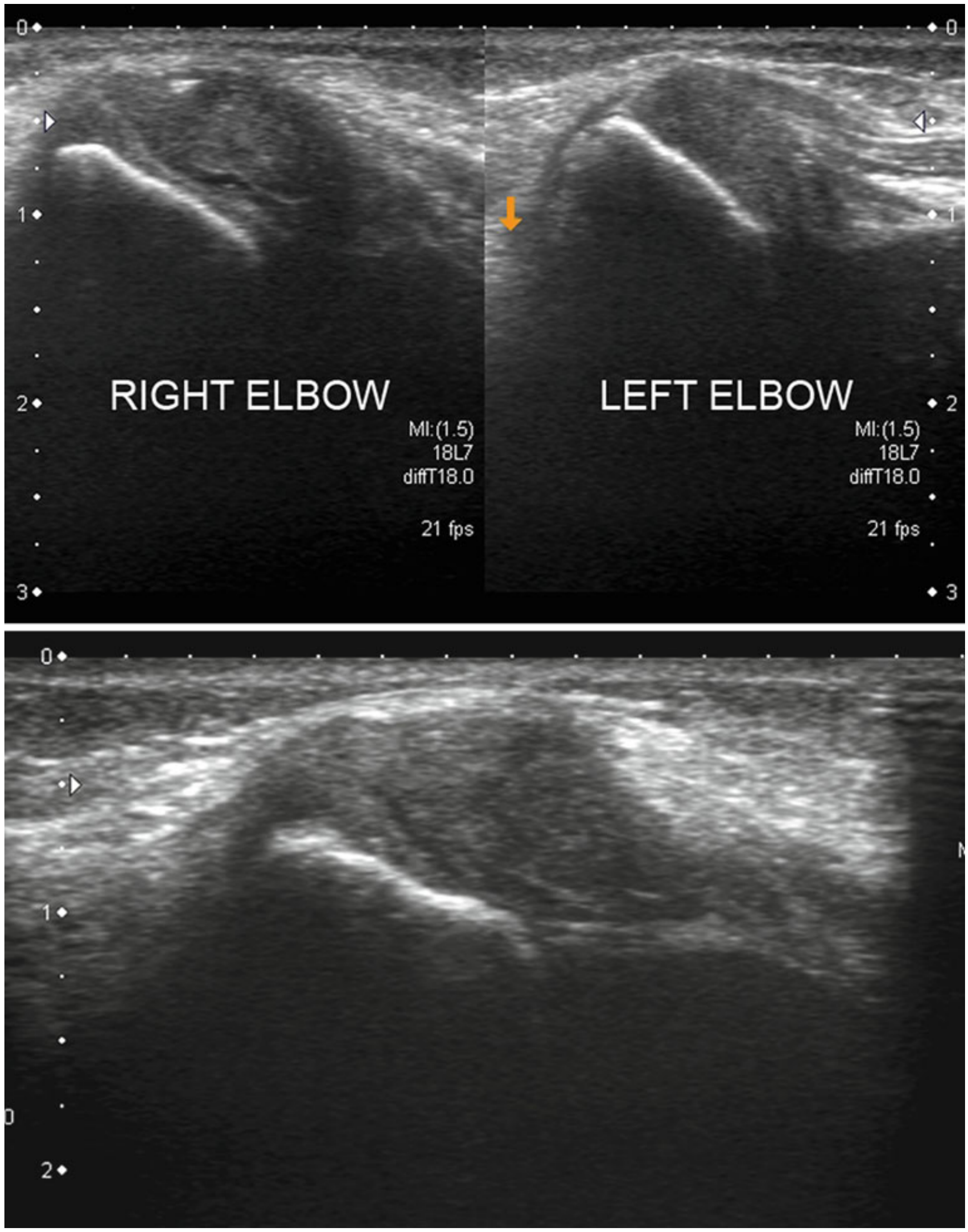

Fig. 9.8 US of a very young child with right-sided avulsion fracture of the non-ossified medial epicondyle of the humerus. The *upper image* shows caudal displacement of the avulsed epicondyle, with hypoechogenic fluid interposed between the fragment and the host cartilage (compare with the normal appearance of the left medial epicondyle). In addition to the above-described avulsion fracture, the *lower image* also discloses a subtle zigzag hypoechogenic fracture line coursing transversely through the cartilaginous fragment

Pediatric fractures may be divided in physeal and non-physeal. Physeal fractures, the main subject of this topic, only occur in the immature skeleton, accounting for 10–30 % of all fractures in children; they raise particular interest because of its potential to cause joint damage and abnormal bone growth. The Salter-Harris classification system is the most widely used, dividing the fractures into five groups according to their location and type of damage to the growth plate, each one of them with distinct prognostic and therapeutic implications (Fig. 9.9). Type I fractures course transversely through the growth cartilage, with no epiphyseal or metaphyseal extension, leading to physeal widening or epiphyseal dislocation (Figs. 9.5, 9.6, and 9.10). Type II fractures are the most common (75 % of all cases), involving the peripheral portion of the metaphysis and part of the growth plate, creating a bone fragment that includes the whole epiphysis and a portion of the metaphysis (Figs. 9.2 and 9.11). Type III lesions are intra-articular fractures that involve the epiphysis and the physis: the fracture line begins in the articular surface, crosses the epiphysis, and presents a transverse component coursing through the peripheral portion of the physis, creating an epiphyseal fragment without connection

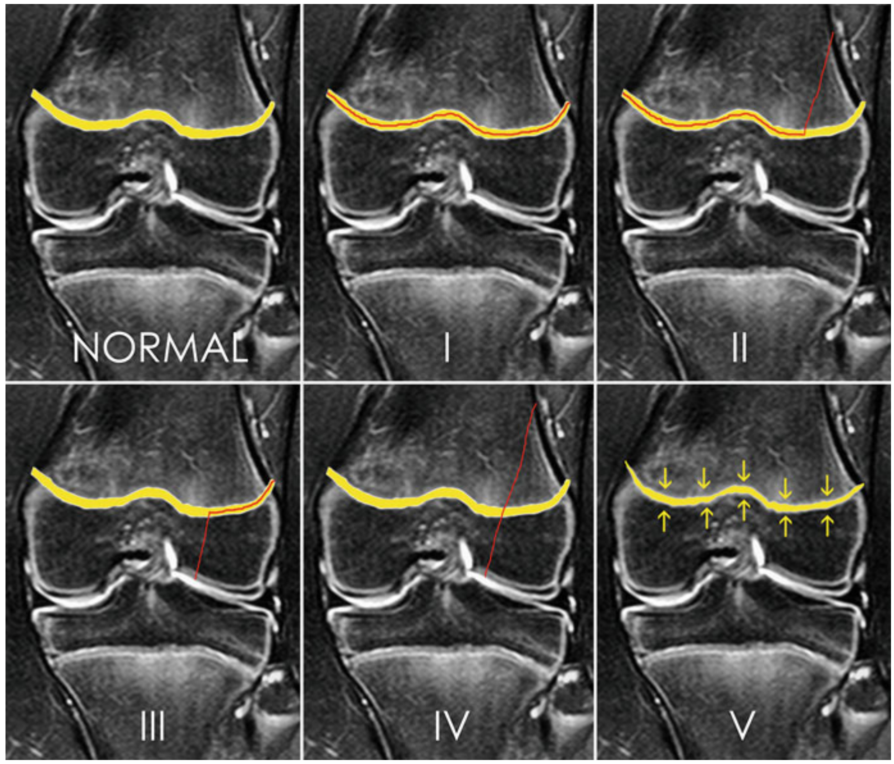

Fig. 9.9 Schematic representation of the Salter-Harris classification for physeal fractures. The physis is represented in yellow and the fracture lines appear in red. While types I and II are physeal and physeal/metaphyseal, respectively, types III and IV are associated with epiphyseal involvement and extend to the joint surface. Type V fracture is a compressive physeal lesion, resulting from the action of axial forces

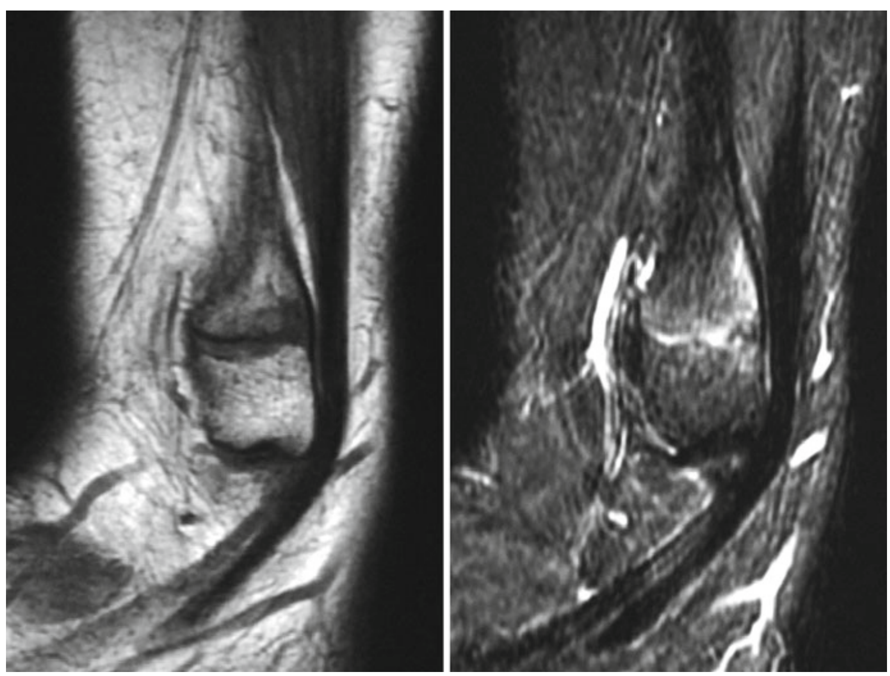

Fig. 9.10 Sagittal T1-WI (*left*) and fat sat T2-WI (*right*) of the right ankle. There is widening of the physis of the distal fibula, more evident on T1-WI, with edematous changes of the physis itself and of the adjacent bone marrow on fat sat T2-WI (Salter-Harris fracture type I)

Fig. 9.11 Lateral (*left image*) and oblique (*right image*) views of the wrist disclosing a physeal/metaphyseal fracture of the distal radius, with dorsal angulation and displacement of the epiphysis and of the metaphyseal fragment

with the metaphysis (Figs. 9.12 and 9.13). Type IV lesions cross the metaphysis and the epiphysis, transecting the physis and the joint surface, therefore producing a bone fragment that includes epiphyseal and metaphyseal components (Fig. 9.7). Type V lesions are the rarest of all (approximately 1 %) and are difficult to diagnose, being caused by axial compressive forces that lead to crushing injury of the physis, without obvious epiphyseal or metaphyseal fractures; radiographs are usually normal or display subtle physeal narrowing. Diagnosis of type V lesions is most often late and retrospective, made after the appearance of complications, such as growth arrest. Generally speaking, type I and type II lesions present good evolution because they do not involve the joint surfaces (Fig. 9.14), while intra-articular lesions (types III and IV) have worse prognosis, with increased risk of secondary osteoarthritis and functional limitation (Figs. 9.4, 9.15, 9.16, and 9.17). Fractures that involve the physis may lead to development of transphyseal bone bridges and/or early physeal closure (Figs. 9.4, 9.16, 9.17, and 9.18). Both MRI and CT are useful in the demonstration of physeal bridges (Fig. 9.4): when centrally located, they tend to cause limb-length discrepancy, while peripheral bridges cause localized growth arrest and angular deformities. In addition to limb shortening, bone bridges may cause damage to the adjacent joints, as well as bowing of the forearm or of the leg if only one of the paired bones is affected (Fig. 9.16). Growth recovery lines that are angled or obliquely oriented – instead of parallel – relative to the physis are indicative of disturbed bone growth related to the presence of bone bars (Fig. 9.16).

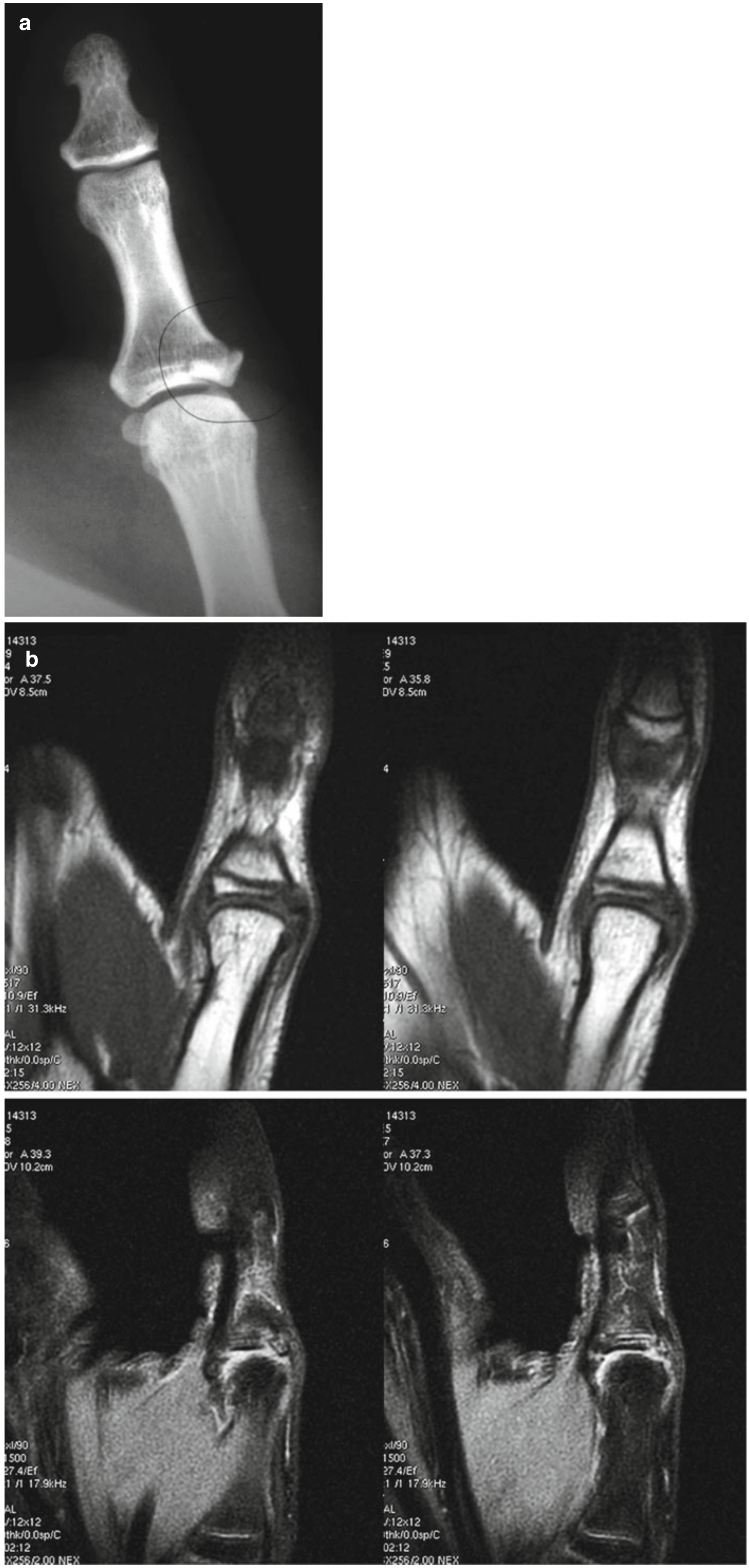

Fig. 9.12 Type III fracture of the base of the proximal phalanx of the thumb in a 14-year-old male. Radiograph (**a**), coronal T1-WI (**b**, *upper row*), and sagittal fat sat PD-WI (**b**, *lower row*) show a mildly displaced physeal/epiphyseal fracture leading to discontinuity of the joint surface

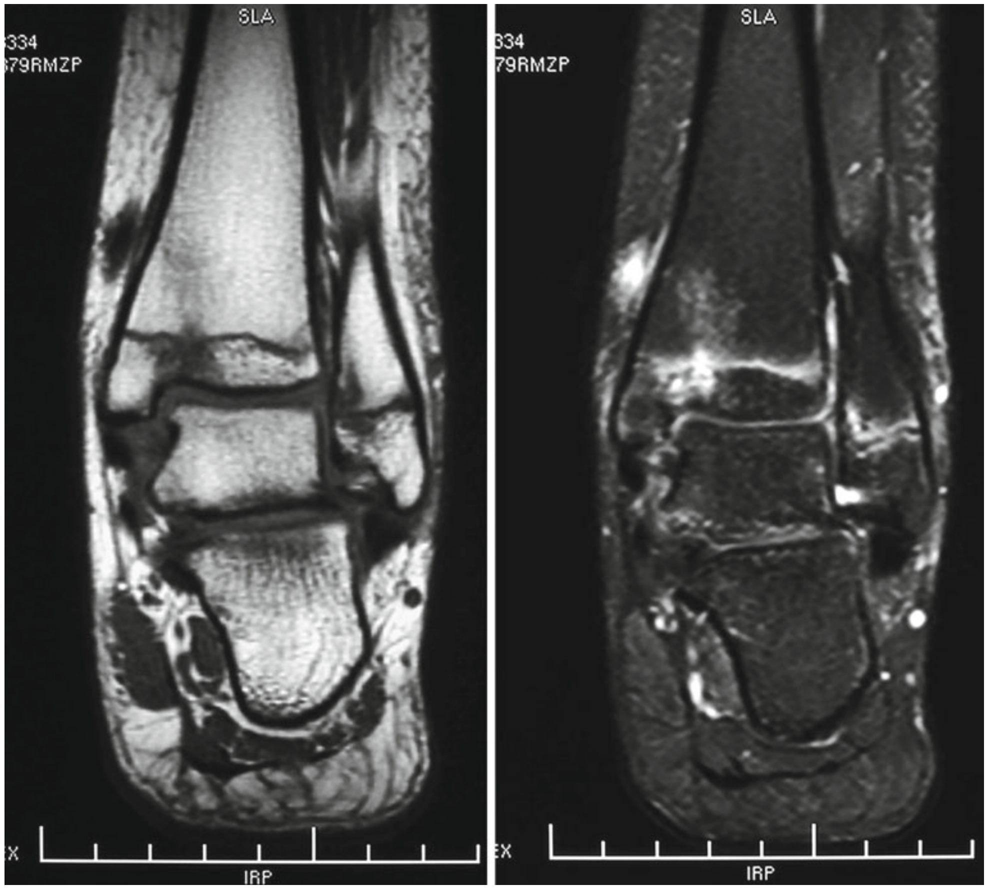

Fig. 9.13 Coronal T1-WI (*left*) and fat sat PD-WI (*right*) of the left ankle of a 12-year-old female demonstrate periphyseal bone marrow edema in the tibia and in the fibula, with a vertical fracture line extending to the joint surface in the medial portion of the tibial epiphysis, also surrounded by marrow edema. These findings are compatible with Salter-Harris fractures type III in the tibia and type I in the fibula

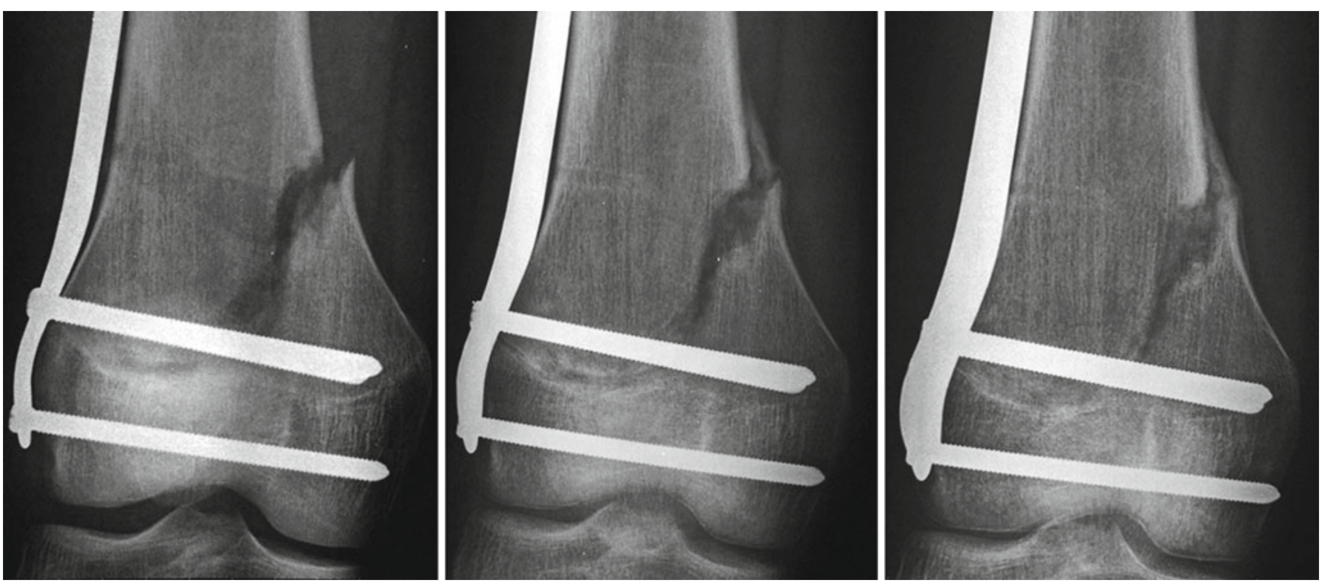

Fig. 9.14 Evolution a type II fracture of the distal femur treated with surgical fixation. Formation of bone callus and progressive healing of the fracture are evident in serial radiographs, with gradual onset of osteoporosis

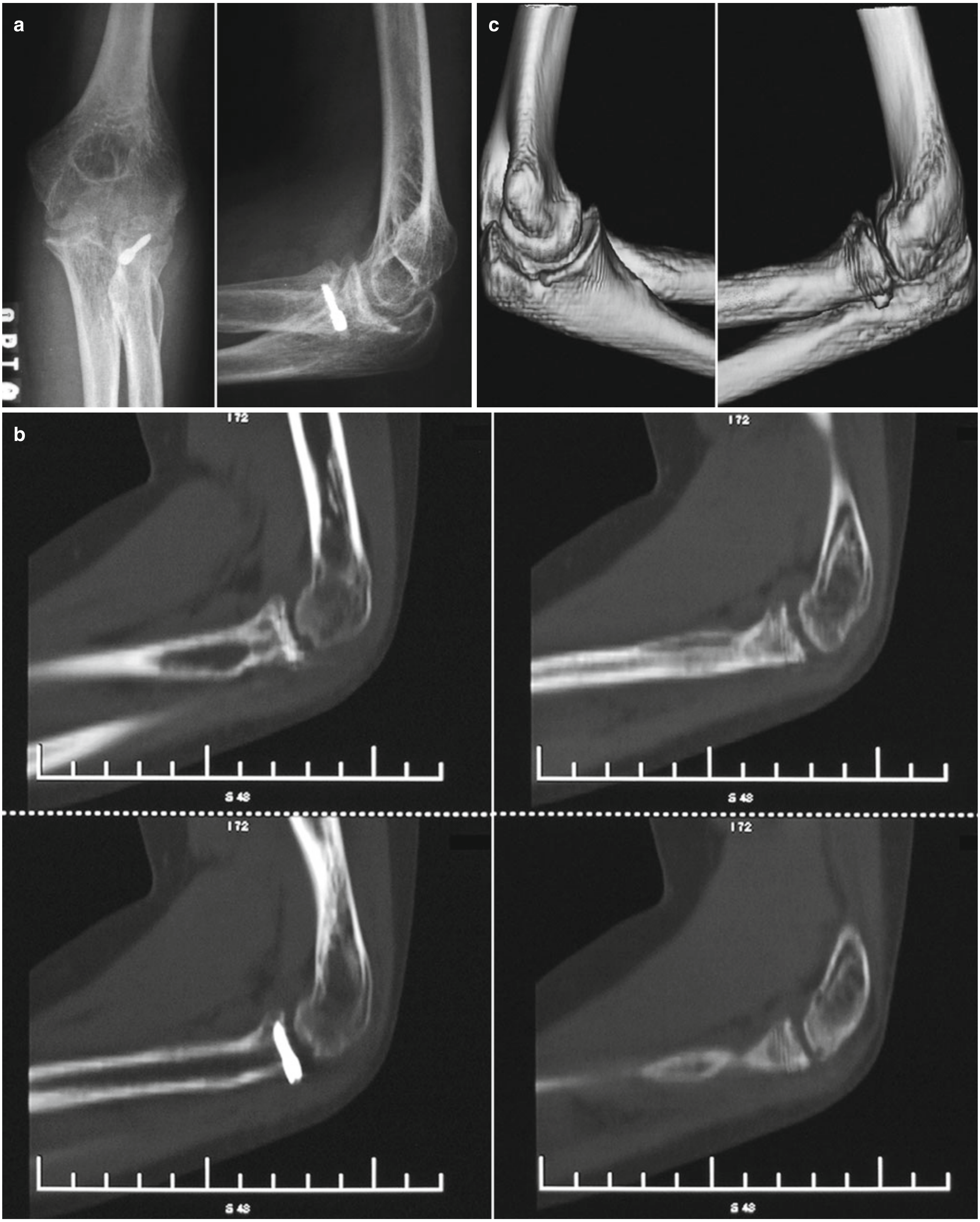

Fig. 9.15 Radiographs (**a**), sagittal reformatted CT images (**b**), and volume-rendered reconstructions (**c**) of an adolescent with sequelae of a surgically corrected elbow fracture. There is irregularity of the joint surfaces, with early-onset osteoarthritis and flexion deformity

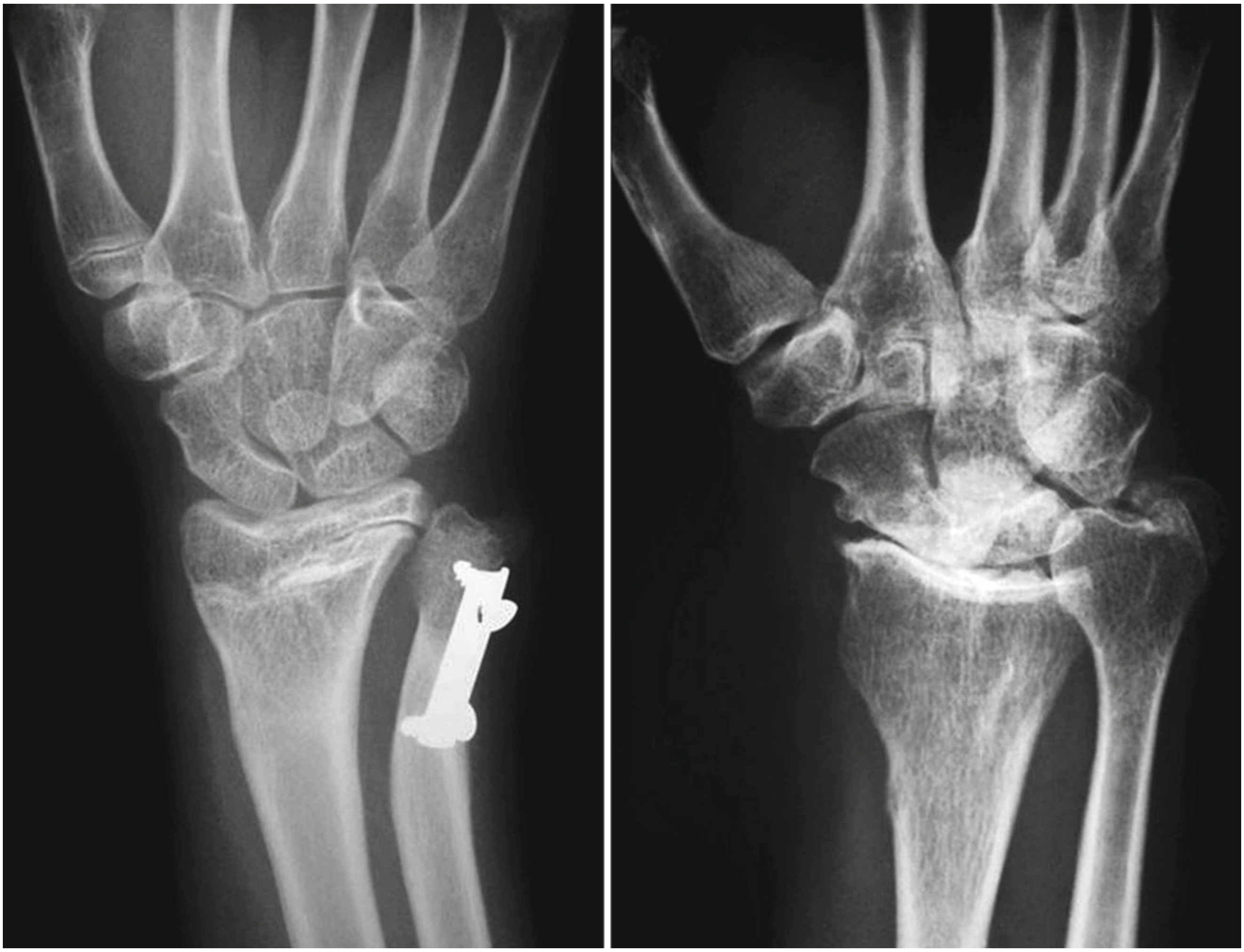

Fig. 9.16 In the *left image*, radiograph of the wrist and of the forearm of a skeletally immature patient demonstrates bowing and residual deformity of the radius and of the ulna, with orthopedic plate and screws in the distal ulna. A peripheral transphyseal bone bridge is seen in the distal radius (to which growth recovery lines converge), as well as incongruity of the radiocarpal joint. At *right*, radiograph of a young adult with sequelae from an old healed fracture of the distal forearm reveals radial shortening (growth arrest related to physeal injury) and premature osteoarthritis of the wrist, as well as deformity of the distal ulna

Fig. 9.17 Old gunshot injury in the head of the fourth metacarpal bone associated with physeal lesion. There is deformity of the metacarpal head and premature physeal closure leading to bone shortening

Some incomplete non-physeal fractures – more frequently found in the distal third of the forearm – will be briefly described as they are typical of the pediatric group. The greenstick fracture is characterized by an incomplete cortical break in the convex edge of the bone and cortical bowing in the concave border, with periosteal apposition that creates a hinge-like effect (Figs. 9.19 and 9.20). Almost one-third of the patients with greenstick fractures will present refractures (which may occur in other types of fracture as well) due to incomplete and/or asymmetric healing (Fig. 9.21). Buckle (torus) fractures present as a subtle cortical irregularity with bulging of the bone surface, typically located adjacent to the metaphyses (Fig. 9.22). The plastic deformation is just an accentuation of the physiological bowing of the affected bone, with no discernible fracture line on radiographs (Figs. 9.21 and 9.23); it is not infrequent for plastic deformation to be associated with other fractures (Fig. 9.21).

Complete diaphyseal fractures are less common in children than in adults (Fig. 9.24). Traumatic osteochondral lesions without fractures are rare in small children and more common in adolescents, usually associated with ligament injuries and joint dislocations, being more frequently found in the talar dome and in the femoral condyles (Figs. 9.25 and 9.26). MRI and CT-arthrography are the only imaging methods able to detect purely chondral lesions, but radiographs and regular non-contrast CT may occasionally disclose fragments of bone attached to displaced osteocartilaginous fragments.

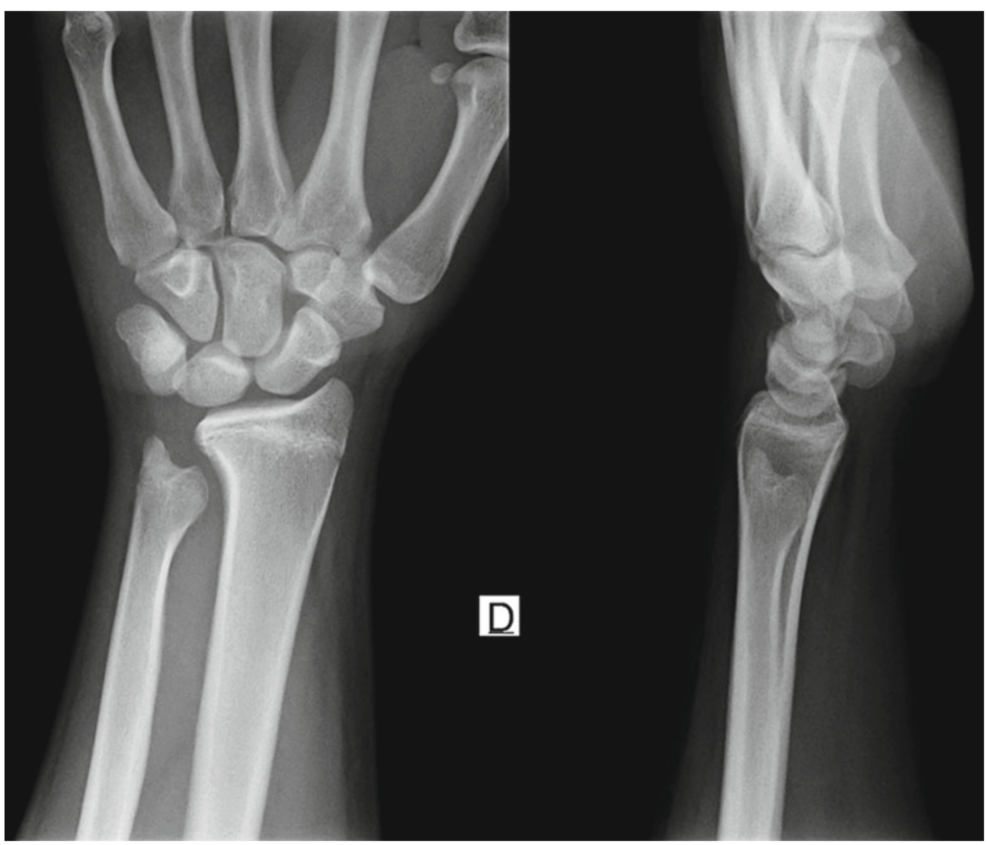

Fig. 9.18 Radiographs of the right wrist and distal forearm of a child with old healed fractures of the homolateral radius and ulna. There is discrepancy in the length of the forearm bones due to early closure of the ulnar physis and, as a consequence, ulnar shortening. Secondary deformity of the distal radius is also present

Fig. 9.19 Sagittal reformatted images (*left*) and volume-rendered reconstructions (*right*) of a CT scan of the forearm of a child demonstrating a greenstick fracture of the distal third of the ulna, with discontinuity of the volar cortex and bending of the opposite side. A complete diaphyseal fracture of the distal radius can be seen in the last image

Fig. 9.20 Radiographs of the distal third of the right forearm of a child who fell on his outstretched hand reveal a subtle incomplete fracture in the lateral cortex of the radius without involvement of the opposite side, as well as mild volar bowing of this bone ("hinge" effect). Greenstick fracture

Fig. 9.21 Radiographs of the right forearm of the same child, taken some months apart. In the *left image*, the first radiograph reveals plastic deformation of the radial mid-diaphysis as well as a subtle incomplete fracture of the lateral cortex of the ulnar mid-diaphysis (more evident in the magnified image) associated with solid periosteal reaction. The follow-up radiograph discloses refracture of the ulna in the same level of the previously described lesion; the fracture complete in the second radiograph, with exuberant bone callus and extensive periosteal reaction. The plastic deformation of the radius remains unchanged

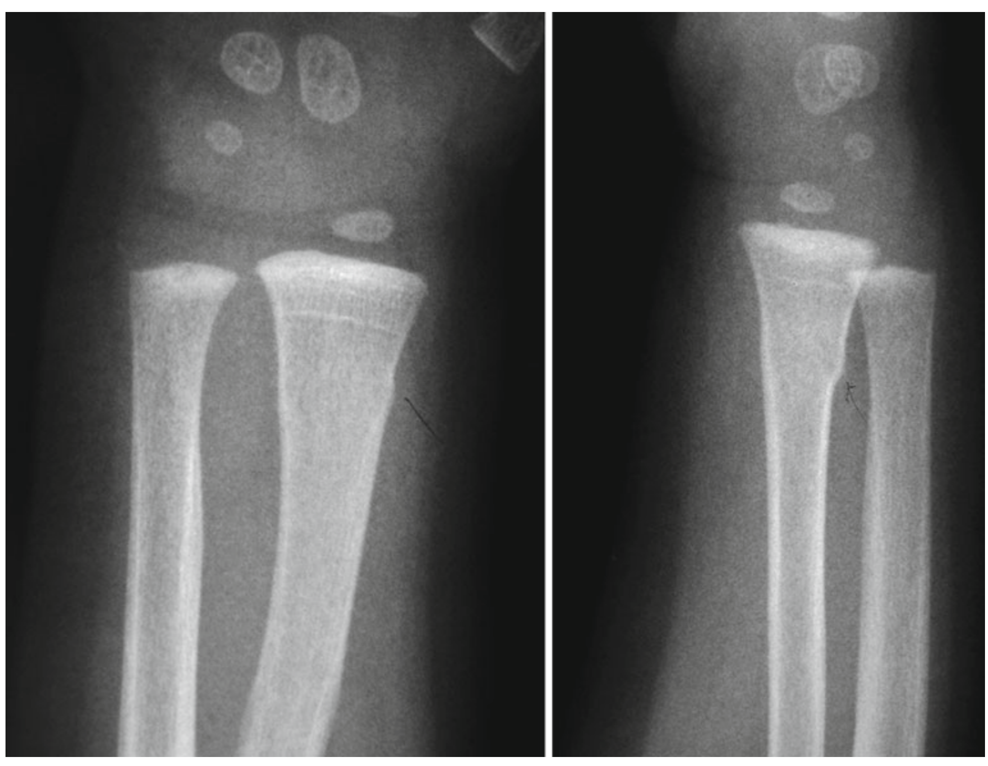

Fig. 9.22 Radiographs of the distal forearm of a young child demonstrate focal bulging in the anterolateral cortex of the distal diaphysis of the radius, typical of a buckle fracture

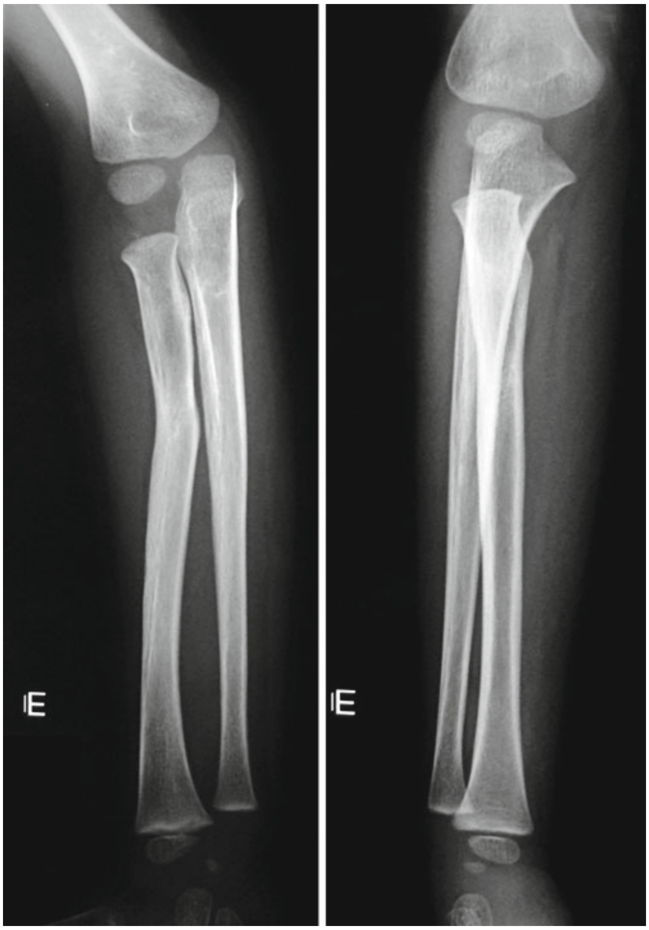

Fig. 9.23 Radiographs of the forearm displaying plastic deformation of the proximal third of the radius, with diaphyseal bowing and absence of cortical discontinuity

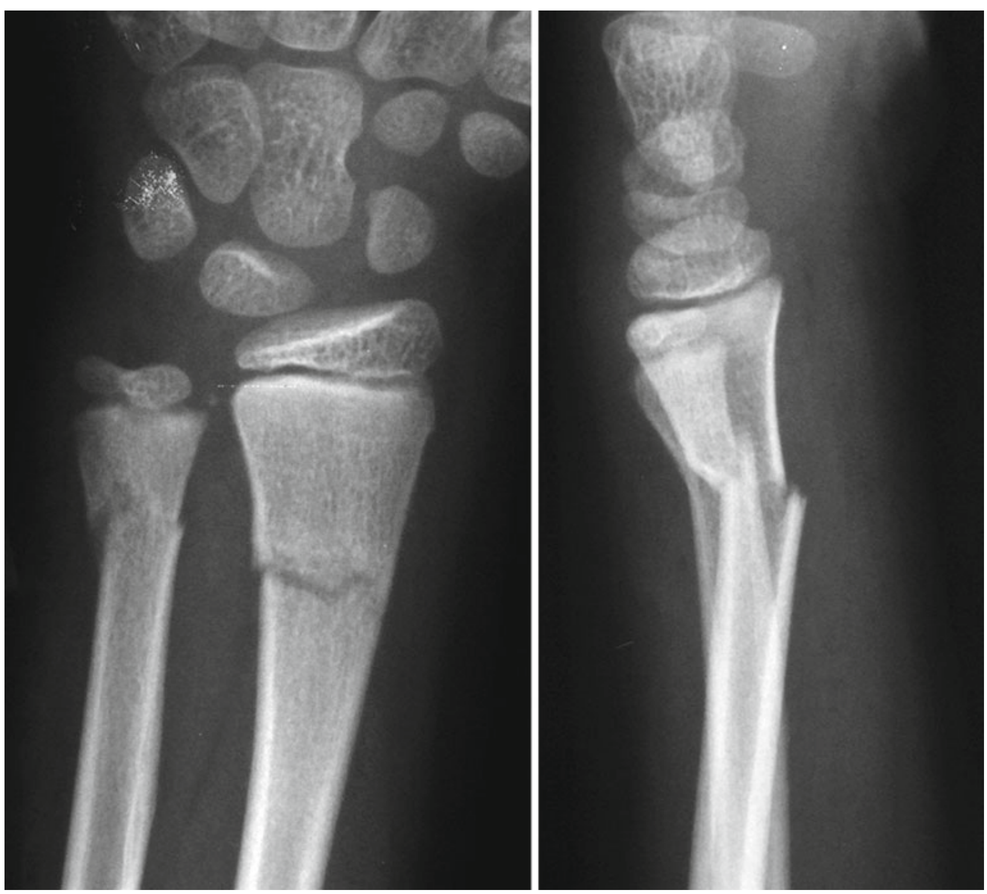

Fig. 9.24 Anteroposterior (*left*) and lateral (*right*) views of the right distal forearm of a child display complete fractures of the distal diaphyses of the radius and of the ulna, with dorsal displacement and angulation of the fragments, leading to the classic "bayonet" deformity. The lateral view is more adequate in estimating the real extent of displacement

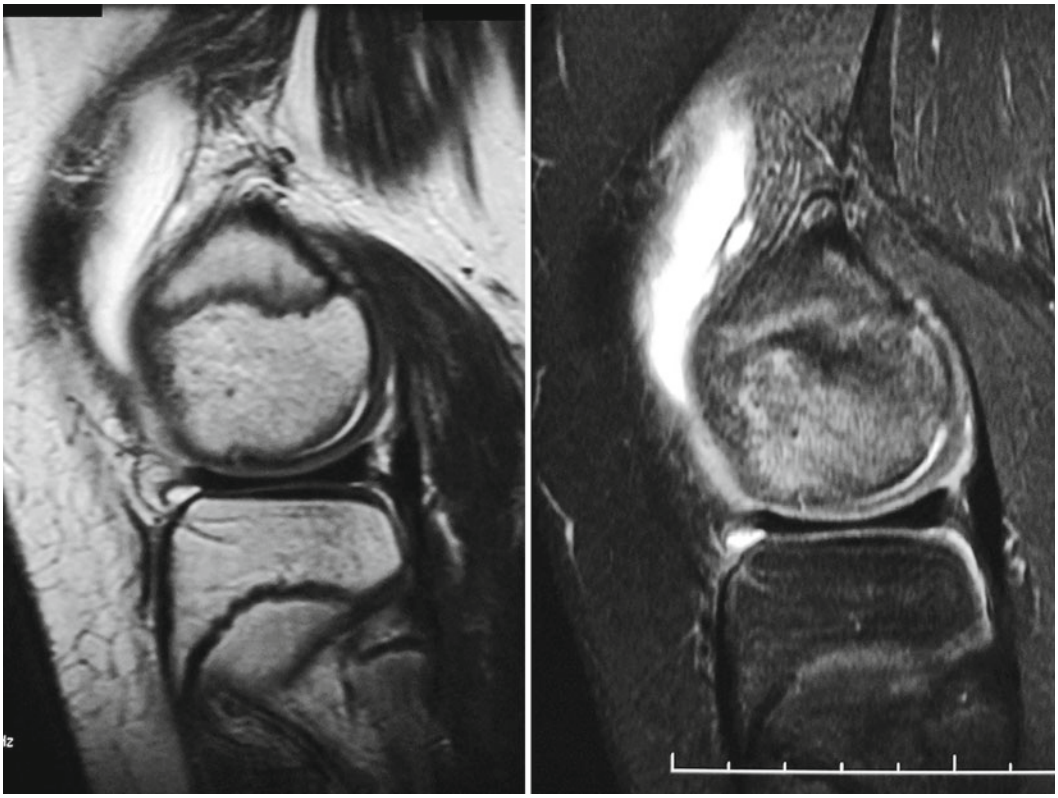

Fig. 9.25 Sagittal T2-WI (*left*) and fat sat PD-WI (*right*) of the left knee of a 13-year-old child at the level of the lateral femoral condyle. There is extensive strip off of the articular cartilage, with fluid in the interface with the subchondral bone, not associated with detachment of cartilaginous fragments. Extensive bone marrow edema pattern is also seen, as well as large joint effusion

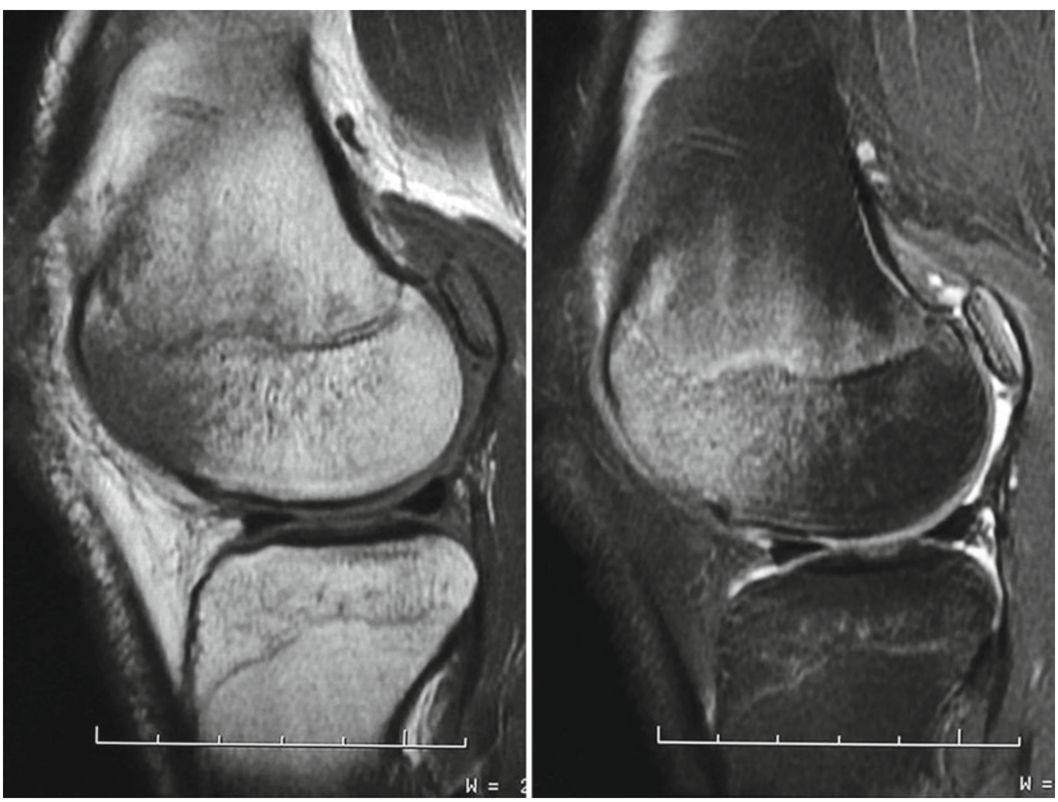

Fig. 9.26 Sagittal T1-WI (*left*) and fat sat PD-WI (*right*) of the right knee of a 17-year-old male with recent trauma evidence detachment of a large cartilaginous fragment from the anterior portion of the medial femoral condyle, with exposure of the subchondral bone and extensive bone marrow edema pattern. The cartilaginous fragment is posterior to the affected condyle and presents signal intensity similar to that of the normal articular cartilage in all sequences

9.3 Pediatric Fractures of the Upper Extremity

The most fractured bone in the shoulder (and in body) is the clavicle, mainly in its middle third (Fig. 9.27). Physeal fractures of the proximal humerus are not common in the pediatric age group, and for the most part are Salter-Harris lesions types I or II. Glenohumeral instability is rare in small children and more frequent in adolescents, presenting as anterior dislocations in more than 90 % of the cases. Classic findings include Hill-Sachs lesion (cortical depression in the posterolateral portion of the humeral head) and Bankart lesion (lesion of the anteroinferior labroligamentous complex, occasionally accompanied by fracture of the adjacent glenoid rim and/or periosteal stripping). MR-arthrography is the preferred imaging method to demonstrate these abnormalities (Fig. 9.28).

The supracondylar fractures and the fractures of the lateral condyle fractures are lesions of the distal humerus that deserve special attention in the pediatric age group. Supracondylar fractures correspond to approximately one-third of the fractures of the extremities in pediatric patients, usually occurring between 5 and 7 years of age. The lateral view is the most important to determine if there is angulation and/or displacement: a line drawn along the anterior cortex of the humerus should intersect the middle third of the capitulum in a normal elbow, but this relation is lost if there is shift – most often posteromedial or posterolateral – of the distal condylar complex (Figs. 9.3 and 9.29). Fractures of the lateral condyle correspond to approximately 20 % of all of fractures of the elbow, occurring more frequently around 4–5 years of life; most lesions are Salter-Harris type IV, following an inferomedial course (Figs. 9.4, 9.7 and 9.30). It may be difficult to distinguish these fractures from joint

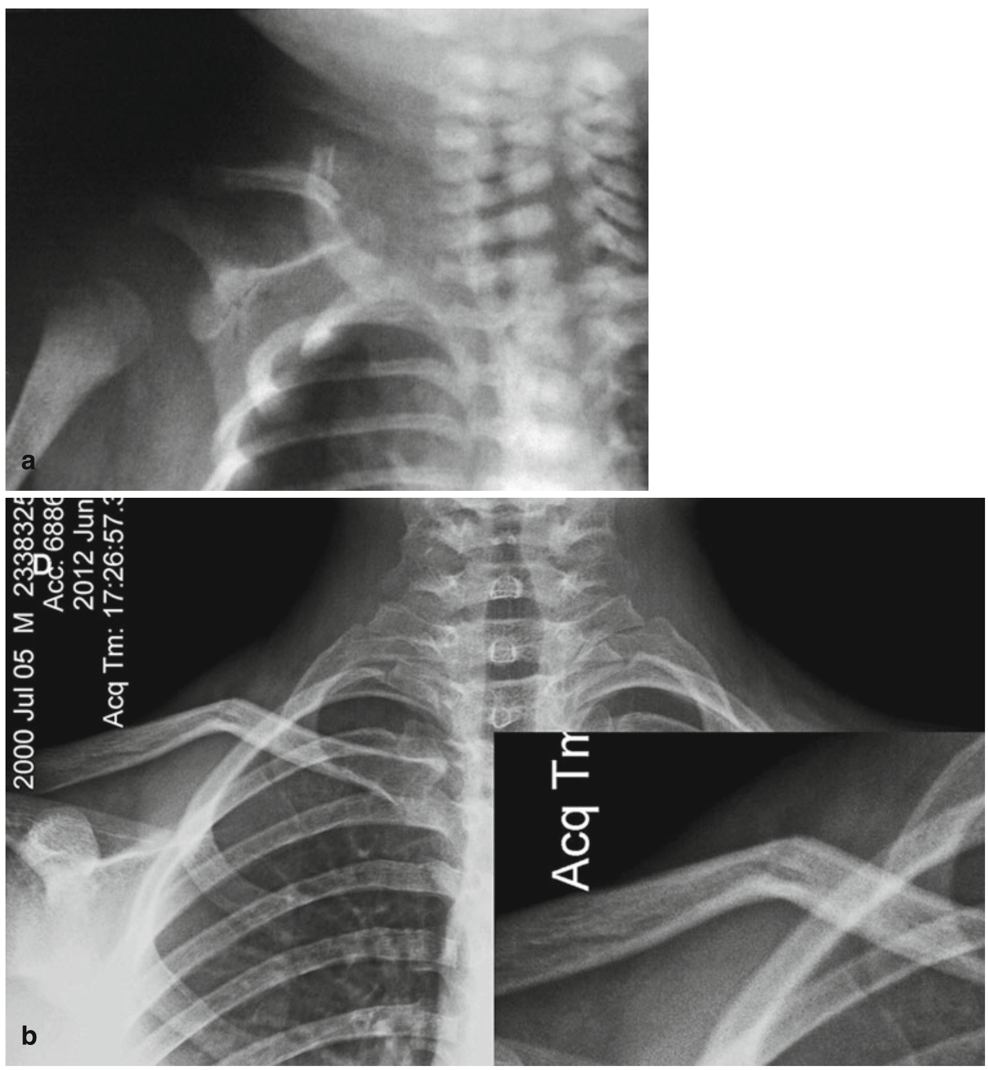

Fig. 9.27 In (**a**), radiograph of a newborn demonstrates complete fracture of the middle third of the right clavicle, with displacement, angulation, and rotation of the medial portion of this bone (birth trauma). In (**b**), radiograph of an 11-year-old child discloses a greenstick fracture of the clavicle, with incomplete cortical disruption in the upper (convex) border and bending of the concave side

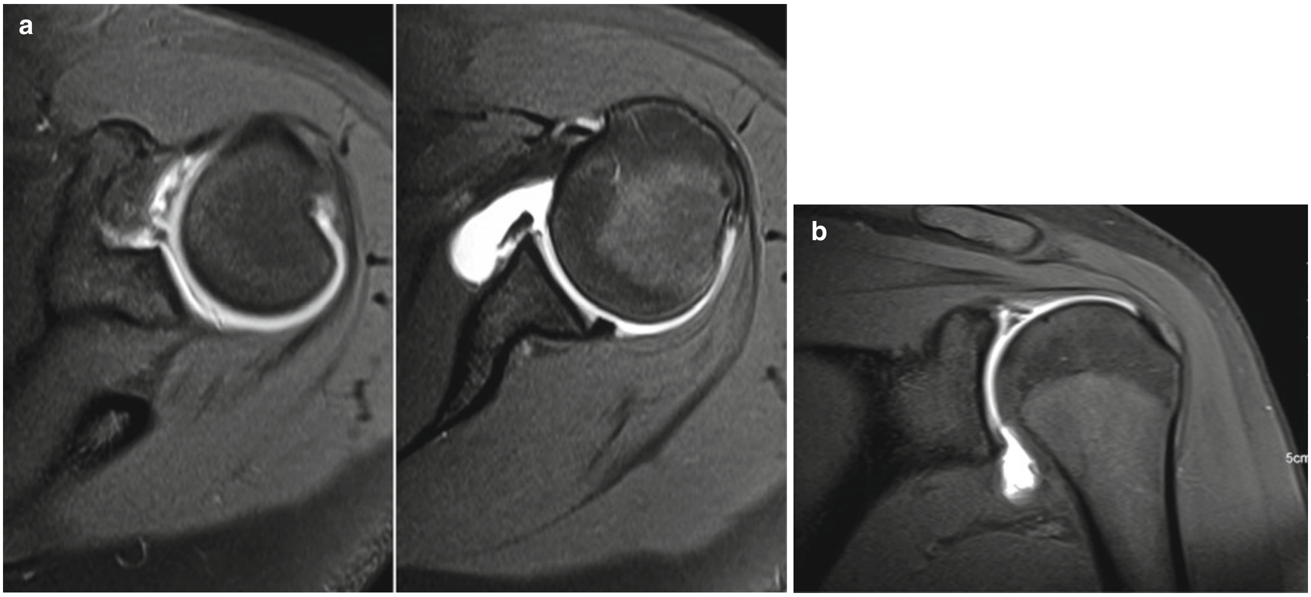

Fig. 9.28 MR-arthrography of the left shoulder of a 16-year-old handball player, performed after an episode of anterior glenohumeral dislocation. Transverse (**a**) and coronal (**b**) fat sat T1-WI demonstrate classic signs of anterior instability, with posterolateral cortical depression of the humeral head (Hill-Sachs lesion) and extensive rupture of the anterior/anterosuperior labrum, as well as avulsion of the adjacent periosteum

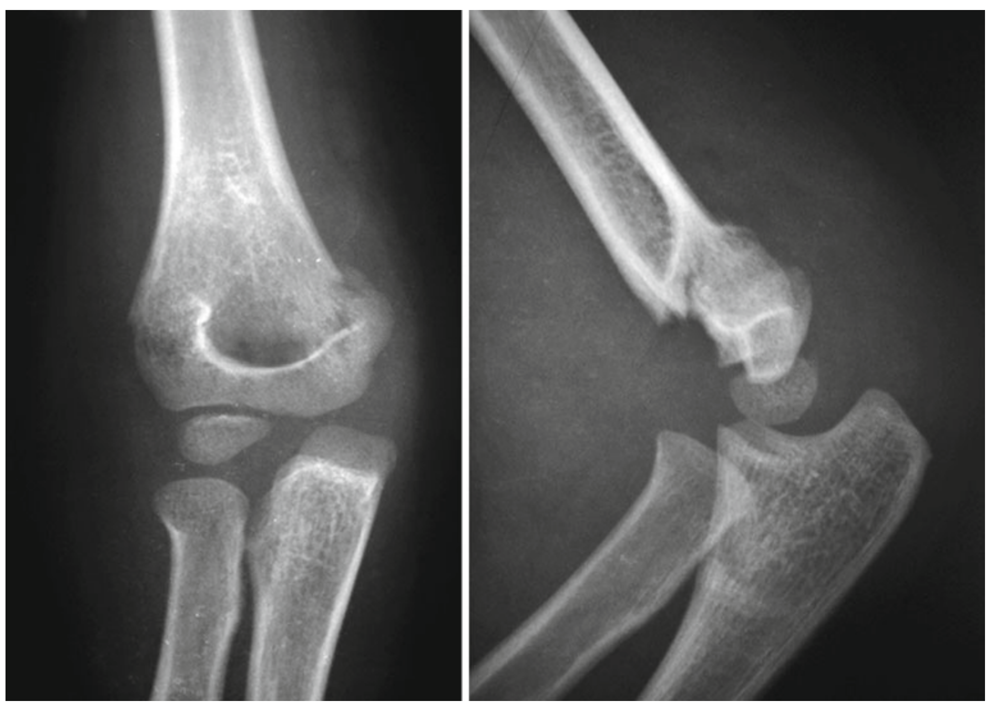

Fig. 9.29 Supracondylar fracture of the humerus. A fracture line is clearly seen in the anteroposterior view, with gross posterior displacement of the distal humerus in the lateral view

dislocations, but in the latter there is loss of the normal relationship between the radial head and the capitulum, which is preserved in fractures. Nonetheless, in small children the capitulum is not yet ossified and radiographic assessment is not feasible, so that MRI and US are useful diagnostic adjuncts in this scenario.

Avulsion of the medial epicondyle is the most important of the avulsion fractures of the ossification centers of the elbow, more prevalent between 7 and 15 years of age; elbow dislocation is associated in up to half of the cases (Figs. 9.8, 9.31, 9.32, and 9.33). The avulsed medial epicondyle may become entrapped within the joint space,

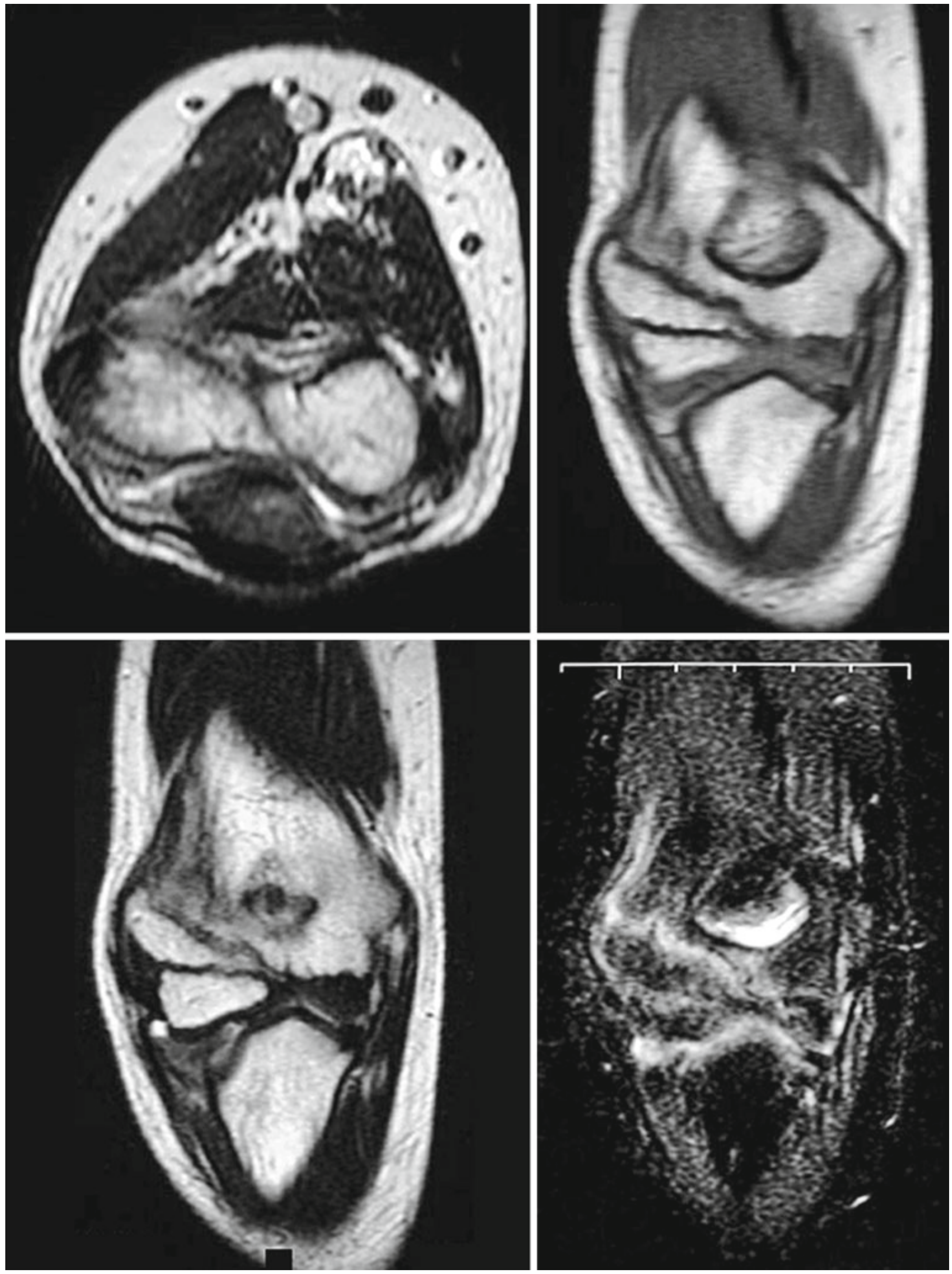

Fig. 9.30 Transverse T2-WI (*upper-left image*) and coronal T1-WI (*upper-right image*), T2-WI (*lower-left image*), and STIR image (*lower-right image*) of the right elbow of a child with a type IV fracture of the lateral condyle of the distal humerus. The fracture line, which is non-displaced and surrounded by bone marrow edema pattern, begins in the lateral cortex of the distal humerus and follows an inferior course, crossing the physis and the non-ossified epiphyseal cartilage

especially if joint dislocation is also present (Fig. 9.32). In small children (under age 6), in whom the ossification center is not yet ossified, radiographs have limited usefulness and intra-articular fragments may appear simply as widening of the medial joint space. US and MRI are often required for proper assessment (Fig. 9.8).

Considering the paired nature of the forearm bones, fracture of one of them is commonly associated with fracture and/or dislocation of the other. Monteggia's fracture, for instance, consists in an association of a fracture of the proximal third of the ulna with dislocation of the radial head (most commonly posterior, which often goes unnoticed), leading to injury of the collateral ligaments of the elbow and of the proximal radioulnar joint (Fig. 9.34). The Galeazzi fracture is a fracture of the distal radius associated with lesion of the distal radioulnar joint. Angulation and displacement are commonly present, leading to radial shortening. In children, there may be separation of the distal ulnar physis instead of injury of the radioulnar joint, a lesion referred to as Galeazzi equivalent.

Fractures of the distal radius are the most common in the pediatric wrist, whether physeal or non-physeal. MRI

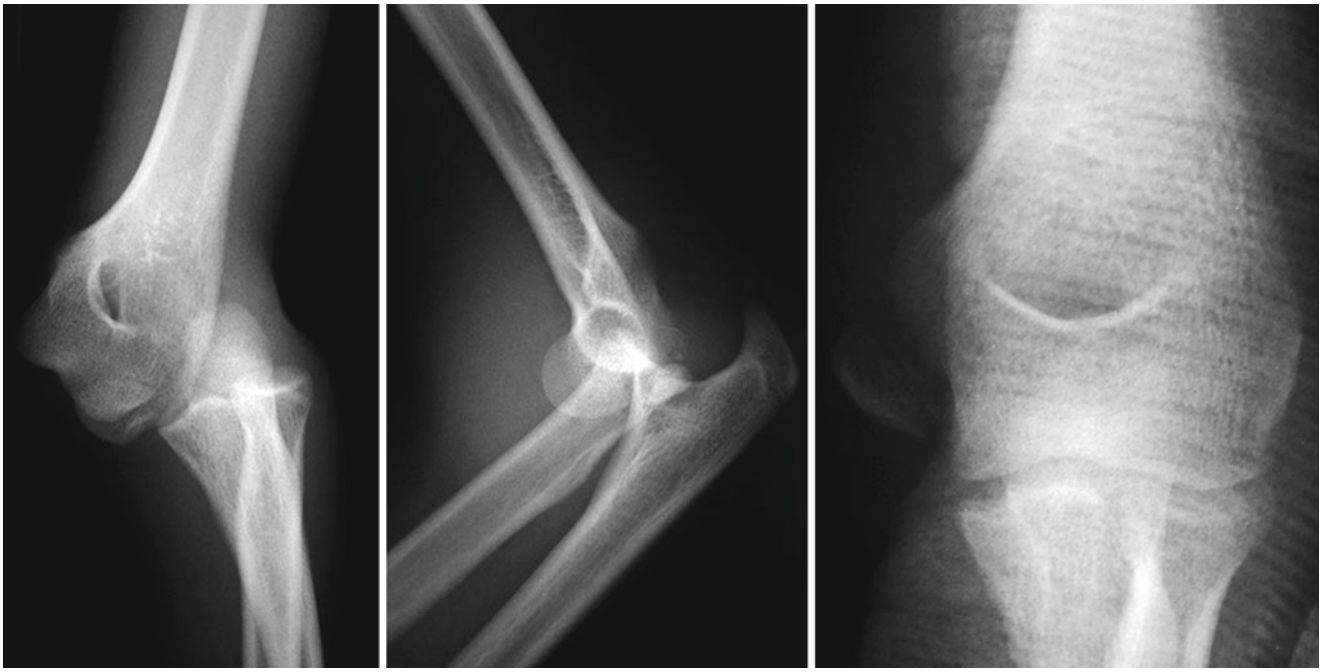

Fig. 9.31 Oblique and lateral radiographs of the left elbow of an adolescent (*left images*) reveal joint dislocation and avulsion of the ossification center of the medial epicondyle, which overlaps the lateral condyle in the *first image* and the coronoid process in the *second one*. The *right image* is an anteroposterior view obtained after reduction that demonstrates the ossification center in its usual position, with obvious physeal widening and subtle bone fragmentation

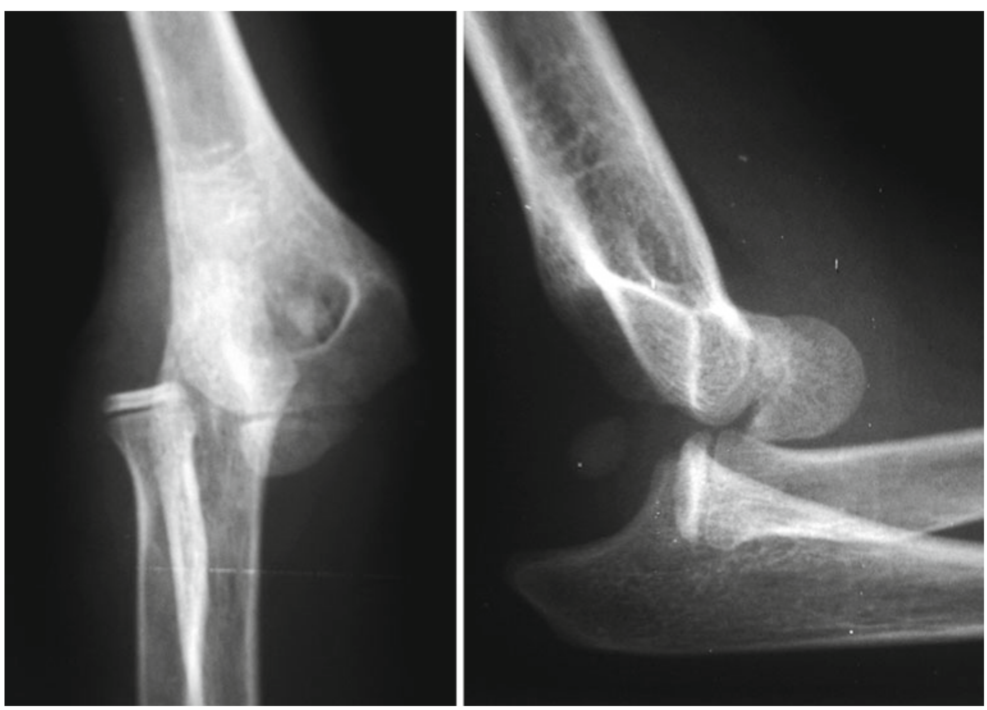

Fig. 9.32 Anteroposterior and lateral radiographs of a child with fracture-dislocation of the right elbow and avulsion of the medial epicondyle. The bone fragment overlies the olecranon fossa in the anteroposterior view, while the lateral view confirms its intra-articular location

Fig. 9.33 MRI of the right elbow of a child with avulsion of the medial epicondyle, coronal and transverse fat sat T2-WI (*upper row*) and T1-WI (*lower row*). The avulsed ossification center, which presents medial displacement and anterior rotation, is attached to the medial collateral ligament, with edematous changes of the bone marrow and of the soft tissues

is especially valuable to diagnose type I fractures (Fig. 9.35) or to detect associated lesions involving soft-tissue structures, such as the triangular fibrocartilage complex or the intrinsic carpal ligaments. Carpal fractures in skeletally immature patients are relatively rare and difficult to diagnose due to the large cartilaginous component of the carpal bones. The scaphoid is the more vulnerable of them, and fractures of this bone are more frequently non-displaced lesions through the distal third, which affect mostly adolescents between the ages of 12 and 15 years (Fig. 9.36). These fractures are frequently undetectable on radiographs; thus, CT and MRI may be useful in difficult cases and the latter is also valuable to detect complications, such as avascular necrosis.

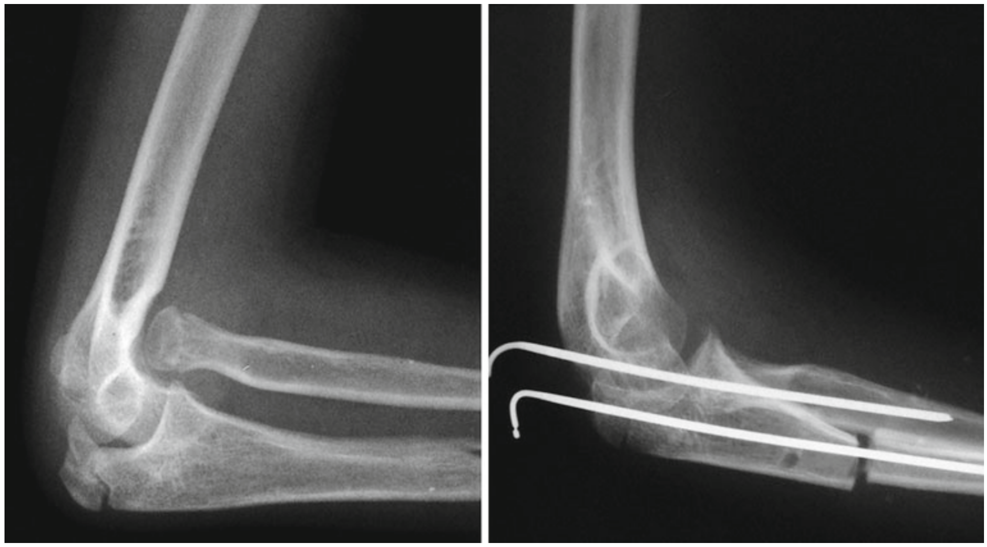

Fig. 9.34 Radiographs of the left elbow and proximal forearm of a patient with Monteggia's fracture performed before (*left*) and after (*right*) surgical correction. It is important to emphasize that the radiograph at left was taken several years after the traumatic event: only the ulnar fracture was diagnosed in the emergency unit and the radial dislocation went unnoticed. There is dislocation of the radial head in the first image, as well as pressure erosion in the anterior cortex of the adjacent humerus, with restoration of its normal relationship with the capitulum in the second image. The fracture of the ulnar diaphysis is partially seen in the first image

Fig. 9.35 Salter-Harris type I fractures. In the *first two images*, coronal T1-WI and gradient-echo image of the wrist of a 13-year-old patient reveal metaphyseal bone marrow edema of the radius and of the ulna, as well as increased signal intensity in the corresponding physes in the second image. Post-gadolinium fat sat T1-WI in the coronal (*third image*) and sagittal (*fourth image*) planes disclose enhancement of the physes and of the edematous bone marrow. Physeal widening is more evident in the dorsal portion of the radius

Fig. 9.36 Transverse (**a**) and coronal (**b**) CT images of the right wrist of a 13-year-old male demonstrate a complete fracture of the scaphoid, with subtle proximal migration of the distal fragment, which is partially interposed between the proximal portion of the scaphoid and the lunate bone, more evident in the coronal plane

9.4 Pediatric Fractures of the Lower Extremity

Hip fractures in children are rare, occurring most frequently in the proximal femur (Fig. 9.37). Posterior hip dislocation and acetabular fractures may be associated, and avascular necrosis of the femoral head is a potential complication. Physeal fractures are relatively uncommon in the knees, which for the most part are Salter-Harris type II lesions (Figs. 9.14 and 9.38); nevertheless, depending on the intensity of the traumatic event, any type of physeal fractures may be found (Figs. 9.5, 9.39, and 9.40).

The most frequent physeal fractures of the ankle are Salter-Harris lesions type I or II of the distal fibula, often associated with partial disruption of the lateral ligaments (Figs. 9.10, 9.13, 9.41, and 9.42). Types II and III lesions of the distal tibia are also relatively frequent (Fig. 9.13). Type IV fractures of the ankle are usually complex, resulting from severe traumatic injuries and more common in the tibia (Fig. 9.43). The triplanar fracture of the distal tibia is a lesion with three components, a sagittal one (coursing through the epiphysis), a horizontal one (through the physis), and a coronal one (through the metaphysis) (Fig. 9.1); CT is especially useful for accurate assessment of complex fractures like this one.

Fig. 9.37 Anteroposterior view of the right hip of a child with a trochanteric fracture of the femur. Pediatric fractures of the proximal femur are rare and usually evident on radiographs.

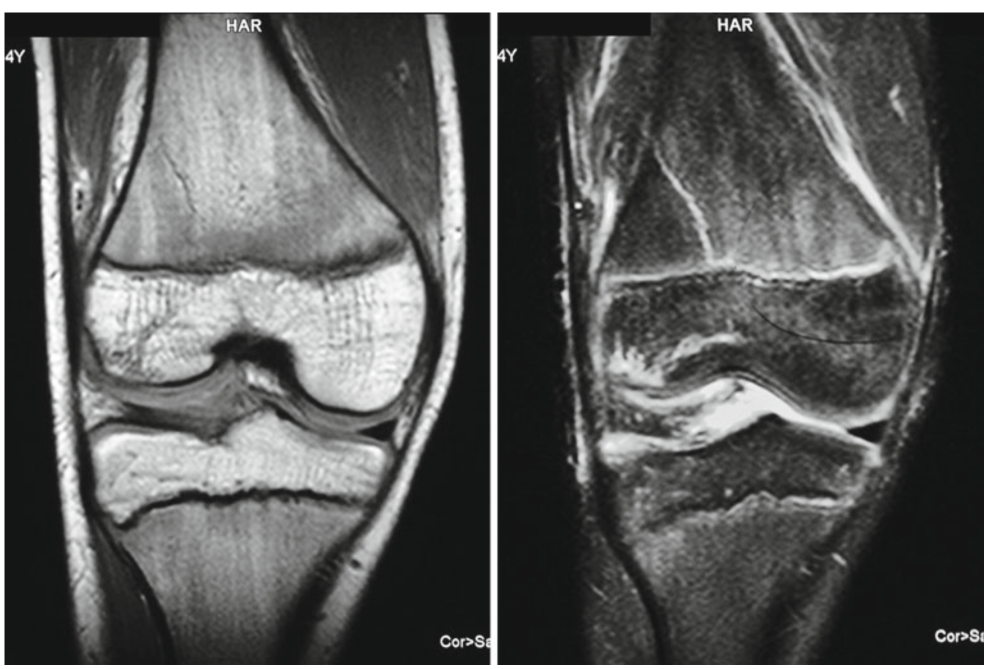

Fig. 9.38 MRI of the left knee of a 14-year-old patient with a Salter-Harris type II fracture of the distal femur. Coronal T1-WI (*left*) and fat sat T2-WI (*right*) disclose an oblique fracture line across the femoral metaphysis, extending from the lateral cortex to the physis. There is obvious physeal widening, medial to the metaphyseal fracture line, representing the horizontal component of the lesion. A subchondral bone bruise is seen on the lateral femoral condyle

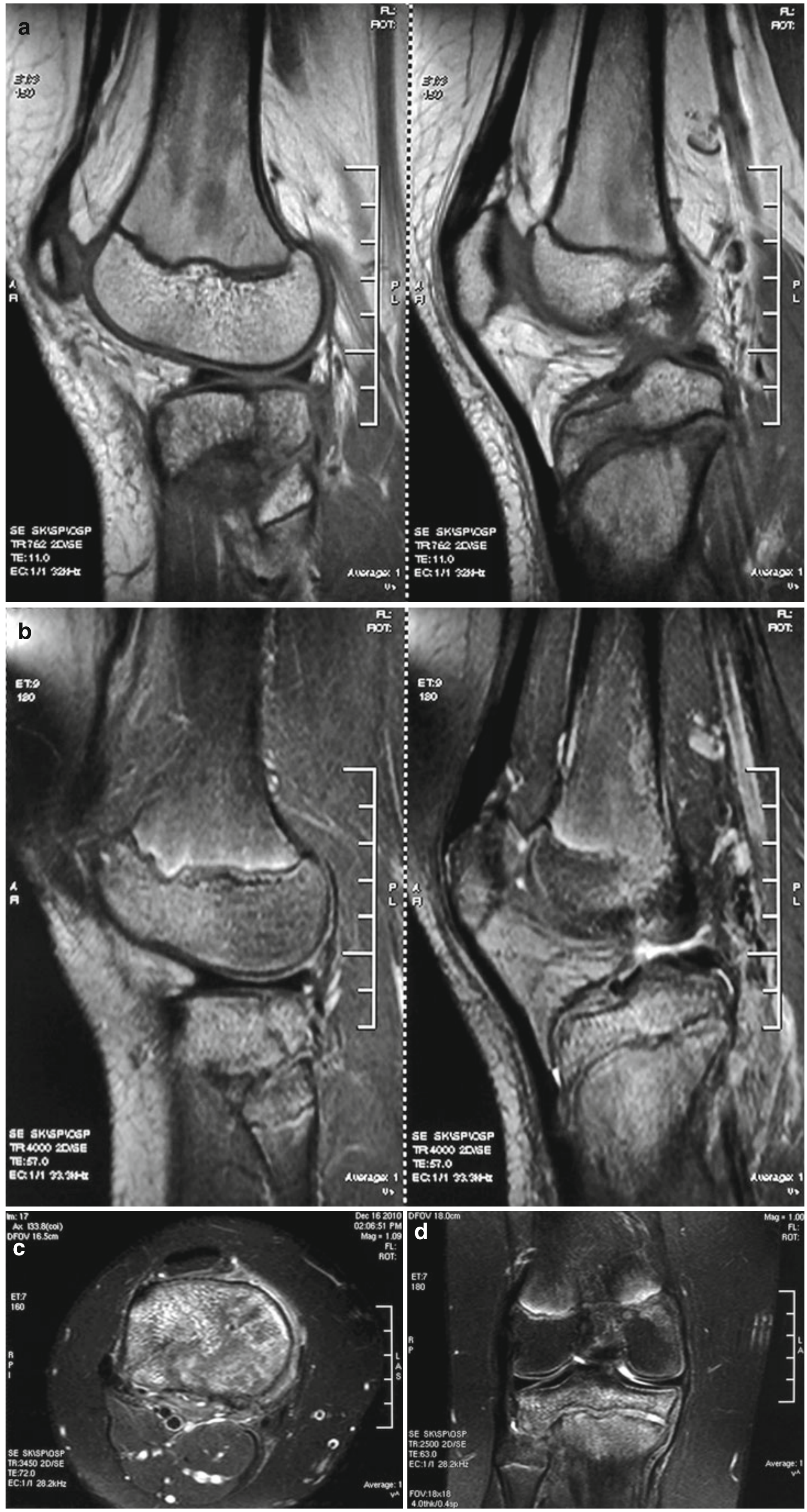

Fig. 9.39 Salter-Harris fracture type III of the proximal tibia. Sagittal T1-WI (**a**) and fat sat T2-WI in the sagittal (**b**), transverse (**c**), and coronal (**d**) planes demonstrate physeal widening associated with a vertical fracture of the tibial epiphysis, in its lateral portion. There is extensive bone marrow edema pattern in the tibial epiphysis and in the metaphysis

Fig. 9.40 Coronal fat sat T2-WI of the left knee disclose a Salter-Harris fracture type IV of the proximal tibia involving the physis and the epiphysis, extending from the proximal metadiaphysis to the articular surface of the lateral plateau. The fracture line is hyperintense, surrounded by bone marrow edema

Fig. 9.41 Salter-Harris fracture type I of the distal fibula. Sagittal T1-WI (*left*) and fat sat PD-WI (*right*) of a 14-year-old patient reveal physeal widening (more evident on T1-WI) and edematous changes of the physis and of the adjacent bone marrow (more evident on fat sat PD-WI)

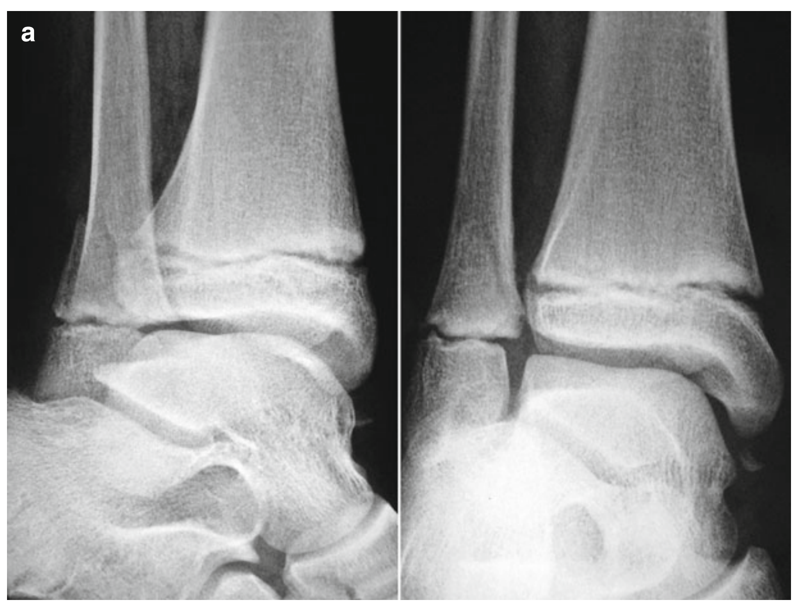

Fig. 9.42 Salter-Harris fracture type II of the distal fibula in an 11-year-old child. Even though a physeal/metaphyseal fracture line is quite evident on oblique views of the ankle (**a**), sagittal T1-WI (**b**, *left*) and fat sat PD-WI (**b**, *right*) demonstrate additional findings, such as marked soft-tissue edema and bone marrow edema pattern

Fig. 9.42 (continued)

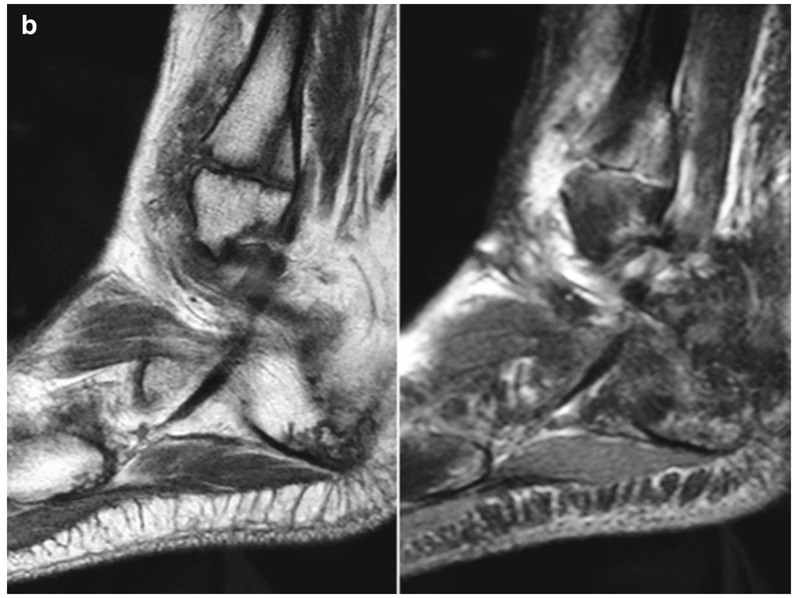

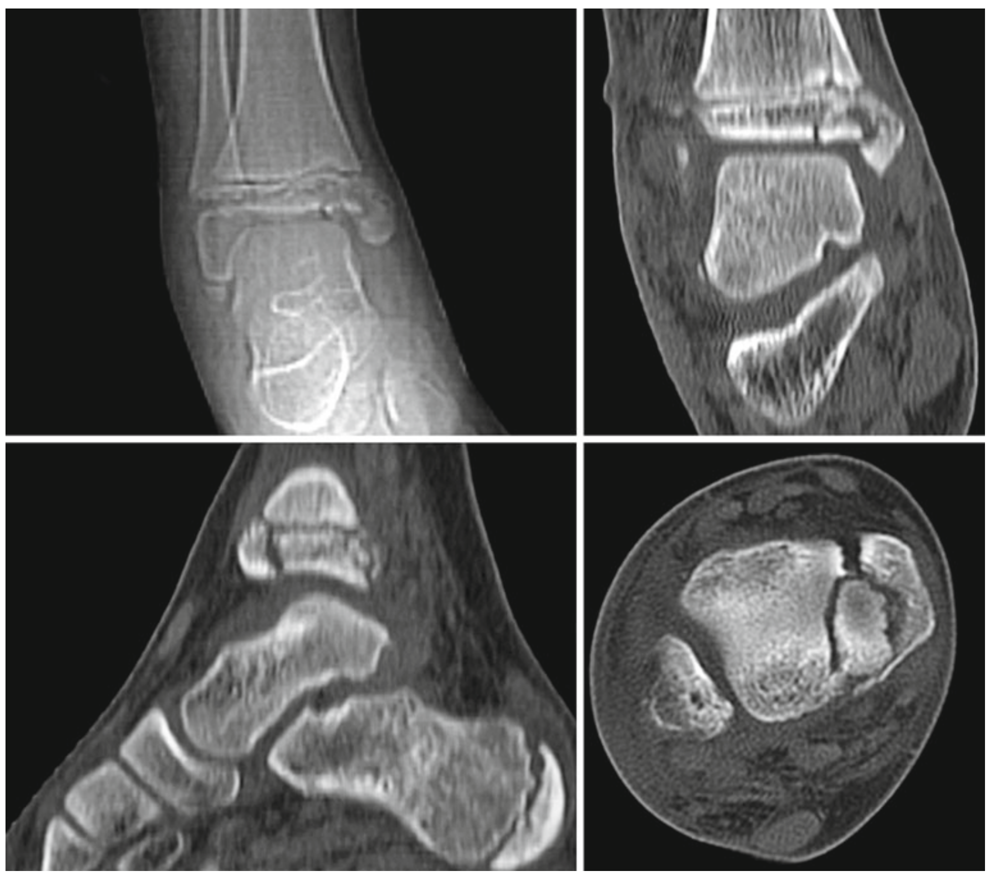

Fig. 9.43 CT scout view (*upper-left image*), reformatted images in the coronal (*upper-right image*) and sagittal (*lower-left image*) planes, and a transverse image (*lower-right image*) of the right ankle of a child who sustained a recent traumatic injury. There is a complex Salter-Harris fracture type IV involving the metaphysis, the physis, and the epiphysis of the tibia, in addition to a fracture of the medial malleolus. CT images are more accurate to demonstrate the real extent of complex fractures like this one

9.5 Traumatic Lesions of the Soft Tissues

Traumatic lesions of the soft tissues in skeletally immature patients are similar to that found in adults on imaging studies. Acute tendon injuries are less frequent and usually less severe in the pediatric group age (Fig. 9.44). Muscle lesions vary from mild strains to high-grade tears. Strains appear on MRI as edematous areas in the affected muscle belly, mostly in the myotendinous junction (Fig. 9.45), while muscle tears present discontinuity of the muscle fibers, either partial or complete, with a hematoma filling the resulting gap. On US, the affected muscle appears heterogeneous, with loss of the normal fibrillar pattern; hypoechogenic material is seen filling muscle tears (Fig. 9.46). Ligaments are more elastic in children and sprains are common, especially in the ankle (Fig. 9.47). Ligament injuries of the knees are relatively infrequent in the pediatric population; however, anterior cruciate ligament (ACL) tears have become more frequent in the last decades as more children and adolescents became engaged in sports practice (Fig. 9.48). In younger children, lesions of the ACL usually involve avulsion of a bone fragment in the tibial insertion (Fig. 9.49). Meniscal tears have also been increasingly reported in skeletally immature patients, and their imaging appearance is similar to that described for adults (Figs. 9.50 and 9.51). Nonetheless, it must be kept in mind that peripheral, transversely oriented linear areas of increased signal intensity in the meniscal substance are common and deprived of significance, probably representing normal vascularity.

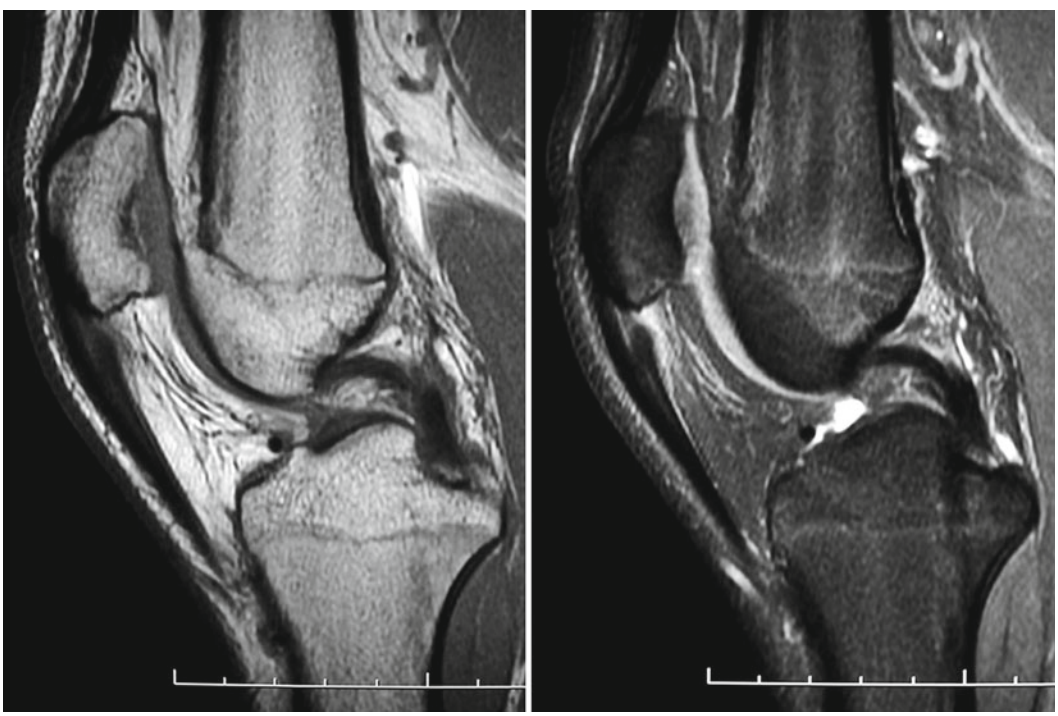

Fig. 9.44 MRI of the right knee of a 16-year-old patient with acute infrapatellar pain during a soccer match. Sagittal T1-WI (*left*) and fat sat PD-WI (*right*) reveal a partial tear of the patellar tendon – which is thickened and heterogeneous – adjacent to its origin, with edema of the Hoffa fat pad and of the bone marrow of the inferior pole of the patella

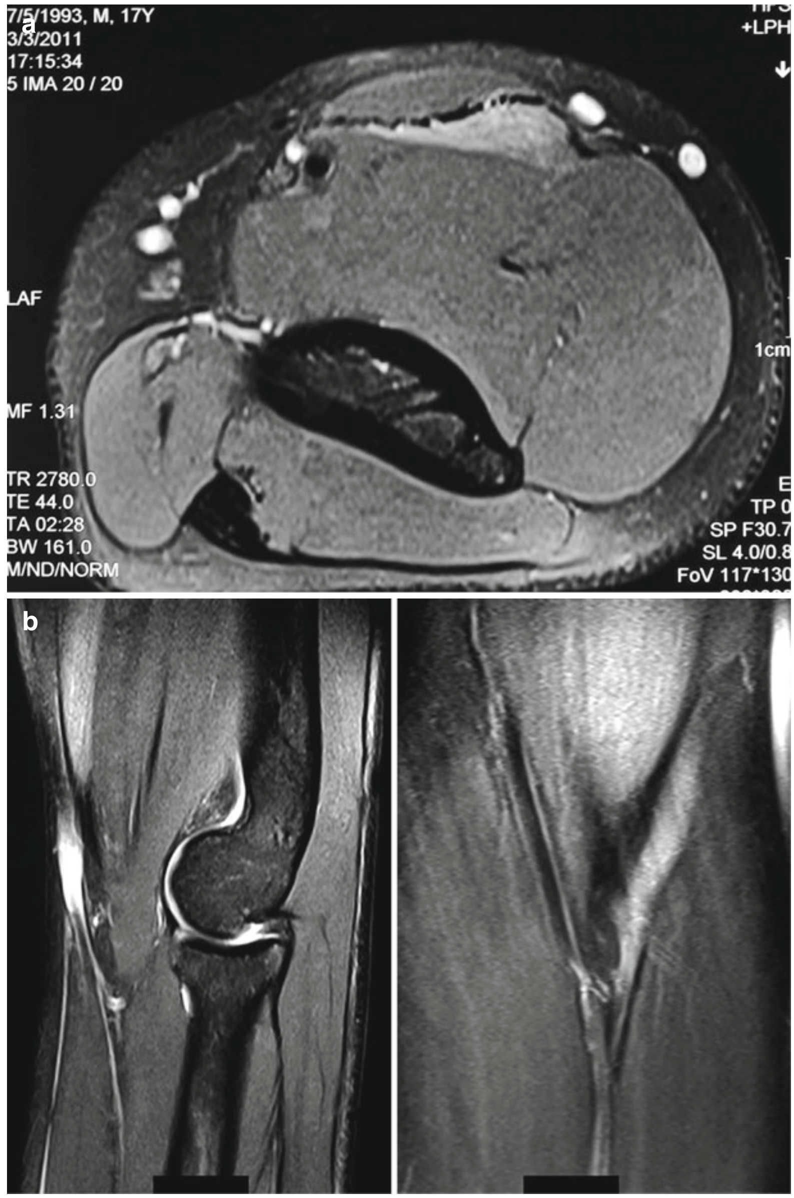

Fig. 9.45 Fat sat PD-WI in the transverse (**a**), sagittal (**b**, *left*), and coronal (**b**, *right*) planes demonstrate edema of the muscle fibers in the distal myotendineous junction of the brachial biceps of a 17-year-old patient, without muscle tear or intramuscular collections, representing a muscle sprain

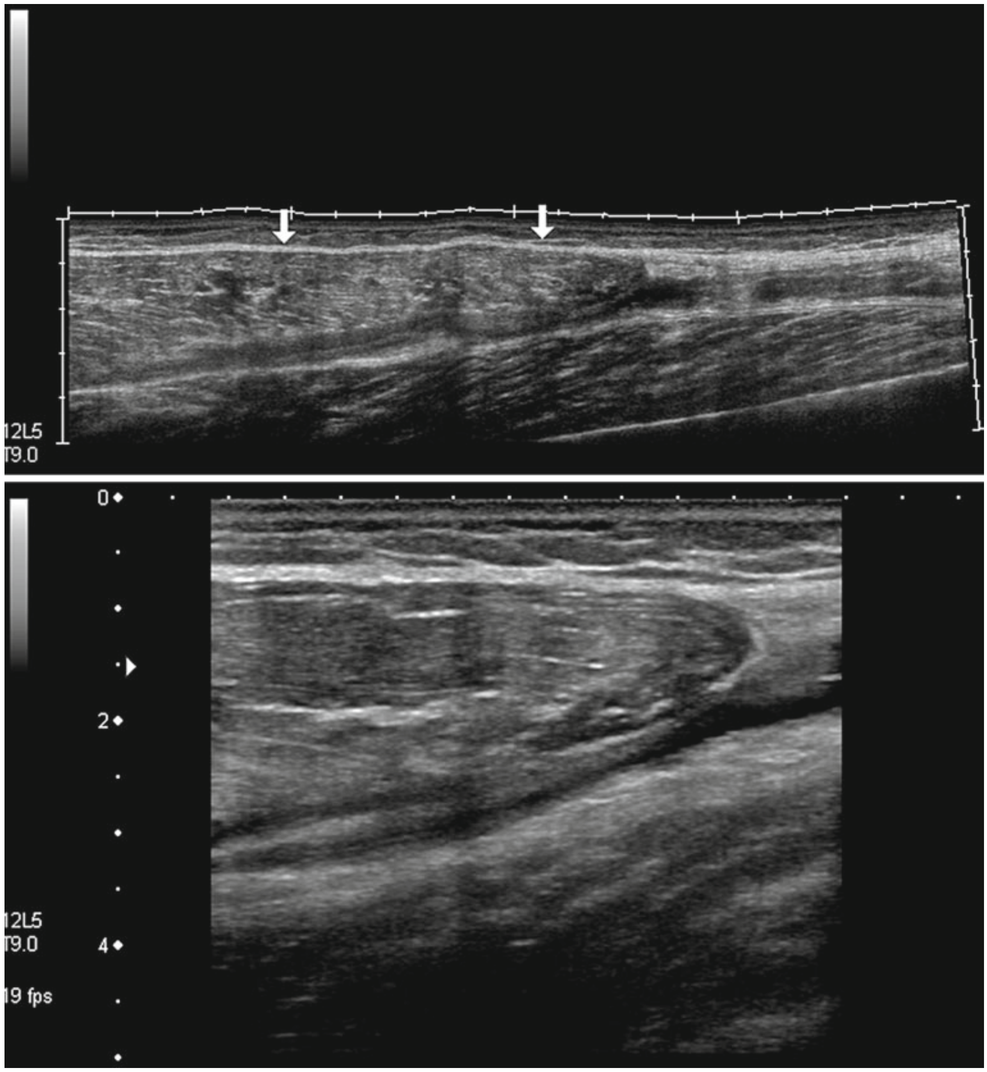

Fig. 9.46 Adolescent with acute pain in the anterior aspect of the right thigh after trauma during a soccer match. The upper image is a longitudinal US scan with extended field of view that demonstrates a complete tear of the rectus femoris, with superior retraction (*arrows*). In the lower image, the inferior portion of the retracted muscle belly is shown in higher detail, with fluid interposed between it and the vastus intermedius

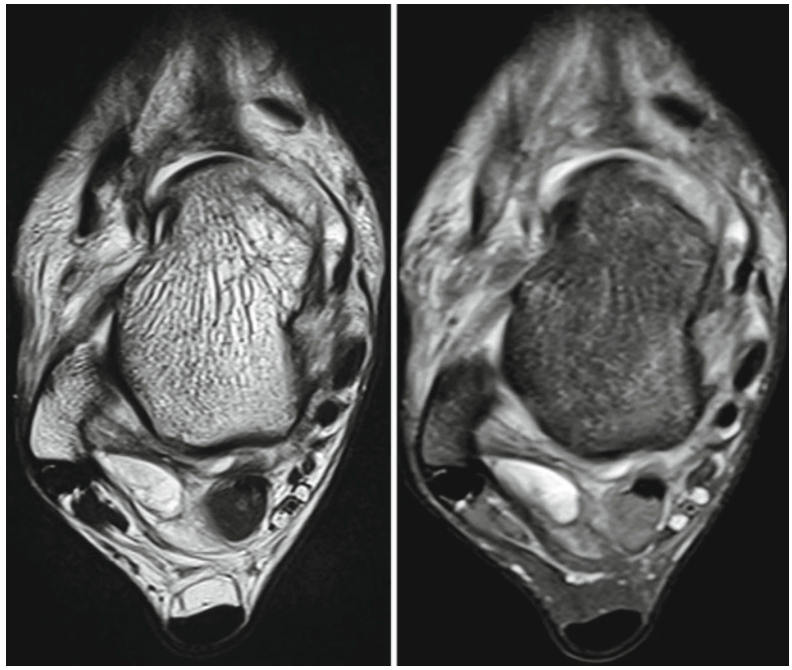

Fig. 9.47 A 15-year-old patient with acute sprain of the right ankle. Transverse T2-WI (*left*) and fat sat PD-WI (*right*) display thickening and heterogeneous signal intensity of the anterior talofibular ligament, without discontinuity of its fibers. Marked edema of the periarticular soft tissues is also seen, as well as joint effusion and fluid in the tendon sheaths

Fig. 9.48 A 16-year-old male seen after knee trauma during a basketball match. Sagittal fat sat PD-WI reveal signs of anterior cruciate ligament tear, including moderate joint effusion, absent visualization of the ligament fibers, typical bone bruises in the lateral femoral condyle and in the lateral tibial plateau, and anterior translation of the tibia. These findings are quite similar to those seen in injuries of the anterior cruciate ligament in adult patients

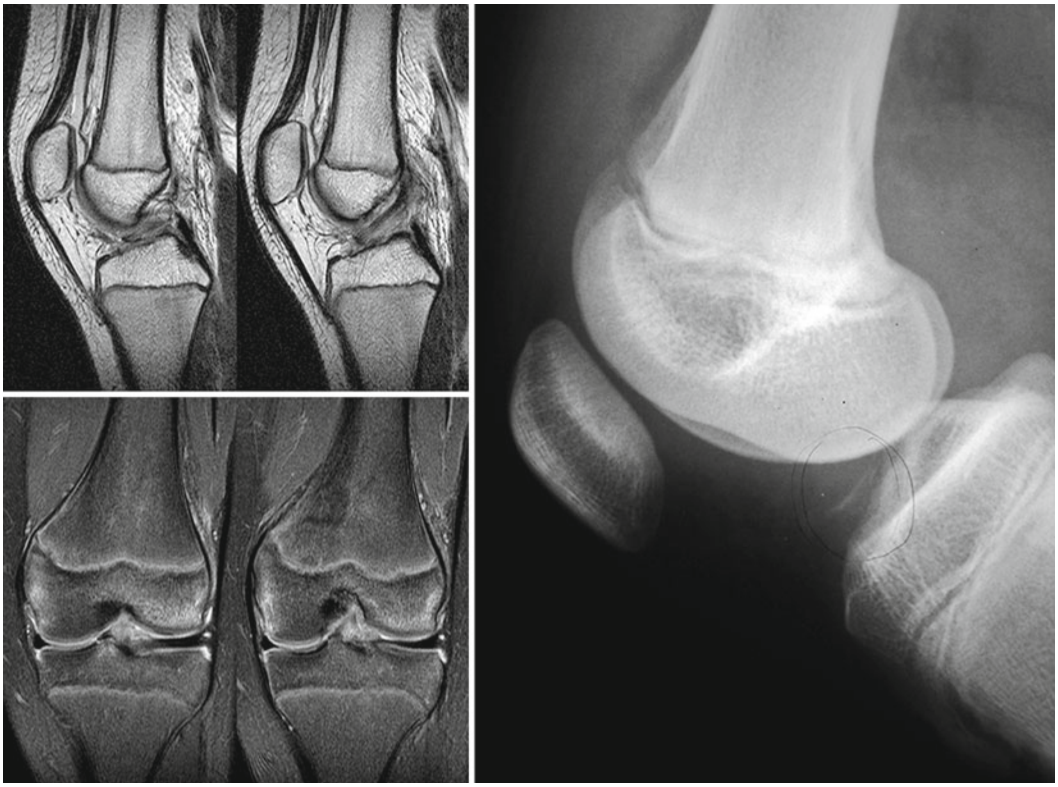

Fig. 9.49 Young child with left knee trauma and clinical evidence of joint instability. At *left*, sagittal T2-WI (*upper row*) and coronal fat sat PD-WI (*lower row*) reveal an intact anterior cruciate ligament. Nonetheless, its tibial insertion is ill-defined, with adjacent bone marrow edema suggesting bone avulsion; subchondral bone marrow edema pattern is also present in the lateral femoral condyle. At *right*, lateral view clearly demonstrates the suspected bone avulsion in the tibial insertion of the anterior cruciate ligament

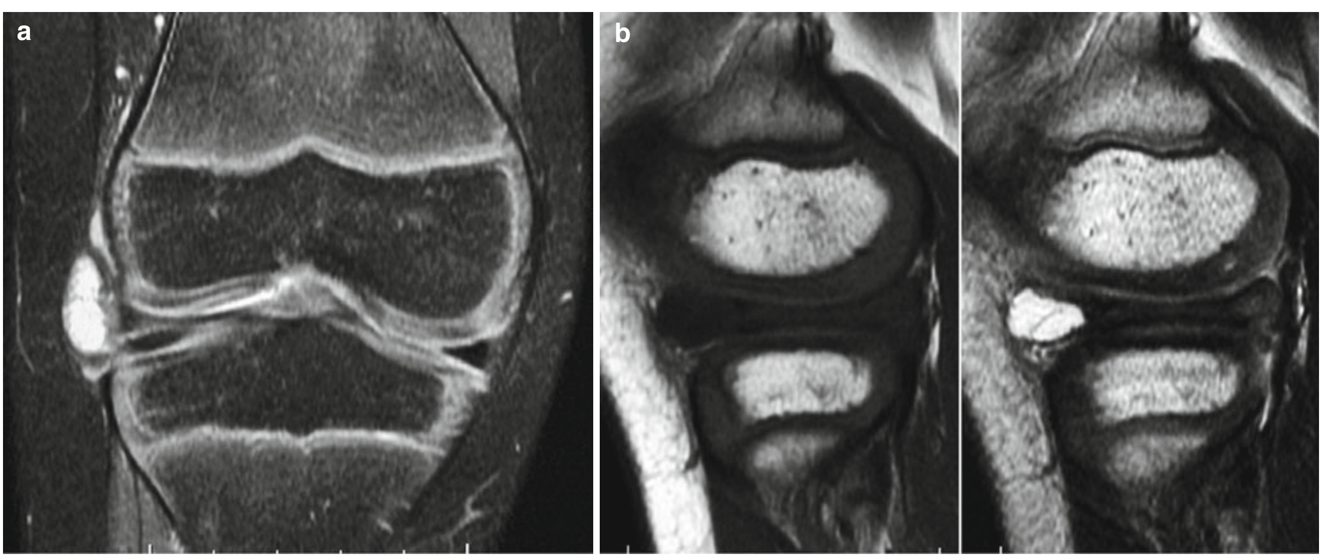

Fig. 9.50 A 6-year-old male with chronic pain in his right knee. Coronal fat sat PD-WI (**a**) and sagittal T1-WI and T2-WI (**b**) disclose a transverse tear across the whole extension of the medial meniscus, with a loculated parameniscal cyst protruding anteriorly and medially. Despite the young age of the child, imaging findings are identical to those of similar lesions seen in adults

Fig. 9.51 Sagittal T1-WI (*left*) and fat sat PD-WI (*right*) of the right knee of a 16-year-old male. There is a vertically oriented full-thickness peripheral tear of the posterior horn of the medial meniscus. Criteria used to diagnose meniscal lesions in children and adults are essentially the same

9.6 Non-accidental Trauma

Physical abuse is a significant cause of morbidity and mortality in the pediatric population, leading to multisystemic abnormalities that include the musculoskeletal system. It is not infrequent for imaging findings to be the first clues to physical abuse, and some patterns of lesion are characteristic enough to suggest the diagnosis. Nevertheless, communication between the radiologist and the attending physician is paramount in order to include child abuse in the differential diagnosis of pediatric trauma, considering all the legal implications. Inexplicable delay in seeking medical attention, inconsistent clinical history, and discrepancy between the severity of the imaging findings and the informed type of lesion are suspicious signs. More than half of all patients will present evidence of skeletal trauma, even though fractures rarely pose a threat to life in abused children.

Radiographs and bone scintigraphy are the most important imaging studies in the investigation of child abuse. The skeletal radiographic survey is a fundamental screening study, as it investigates each anatomic site separately, including the axial and the appendicular skeleton. An additional survey performed 14 days later may disclose periosteal neoformation and fractures that were not evident previously. Radiographs are able to distinguish recent lesions from old fractures, an important feature as injuries are recurrent in these patients. The overwhelming majority of the fractures in abused children occur before 18 months of life, while most of the accidental osteoarticular lesions take place after age 5. Bone scintigraphy can evidence even subtle fractures or areas of periosteal detachment, but it is limited to demonstrate the classic metaphyseal lesions (see below) or skull fractures. The role of CT in musculoskeletal evaluation of child abuse is limited and it is mostly used as an adjunct to clarify equivocal radiographic findings. MRI and US are only exceptionally used and do not have an established role in this context.

The most important radiographic findings include multiple fractures in different stages of healing, old fractures left untreated (with hypertrophic callus and lack of consolidation), and several areas of periosteal apposition in the metaphyses of the long bones (related to posttraumatic bleeding) (Figs. 9.52 and 9.53). Even though there are no pathognomonic lesions, some patterns of lesion present a high degree of specificity for child abuse. Multiple rib fractures, for instance, mainly when bilateral and symmetric, are very suggestive. The classic metaphyseal lesion (corner fracture) is also highly specific in small children: it is a peripheral fracture of the metaphysis, with a triangular or bucket-handle appearance, representing avulsion of the periosteum and of the immature bone (Fig. 9.53). Corner fractures are more common in the long bones around the shoulders, knees, and ankles. Diaphyseal fractures of the long bones are the most common fractures in physically abused children; spiral or oblique diaphyseal fractures in children with less than 1 year of age present a higher degree of specificity (Fig. 9.53). Epiphyseal separations are strongly associated with child abuse, notably in the distal humerus (Fig. 9.53), even though Salter-Harris fractures are relatively uncommon. Scapular and sternal lesions in small children should also be considered secondary to non-accidental trauma unless proven otherwise (Fig. 9.52). Compressive fractures of the vertebral bodies are more common in the thoracolumbar transition, and fractures of the spinous processes are also very suggestive. In skull fractures, evidence of high-energy traumatic injuries without a compatible clinical history must raise the possibility of physical abuse (Fig. 9.53). The most important condition to be considered in the differential diagnosis is osteogenesis imperfecta, in which, in addition to multiple fractures, there are marked osteoporosis and a larger than usual number of Wormian bones. The clinical history, the physical examination, and a careful analysis of the radiographs usually allow safe differentiation between osteogenesis imperfecta and child abuse.

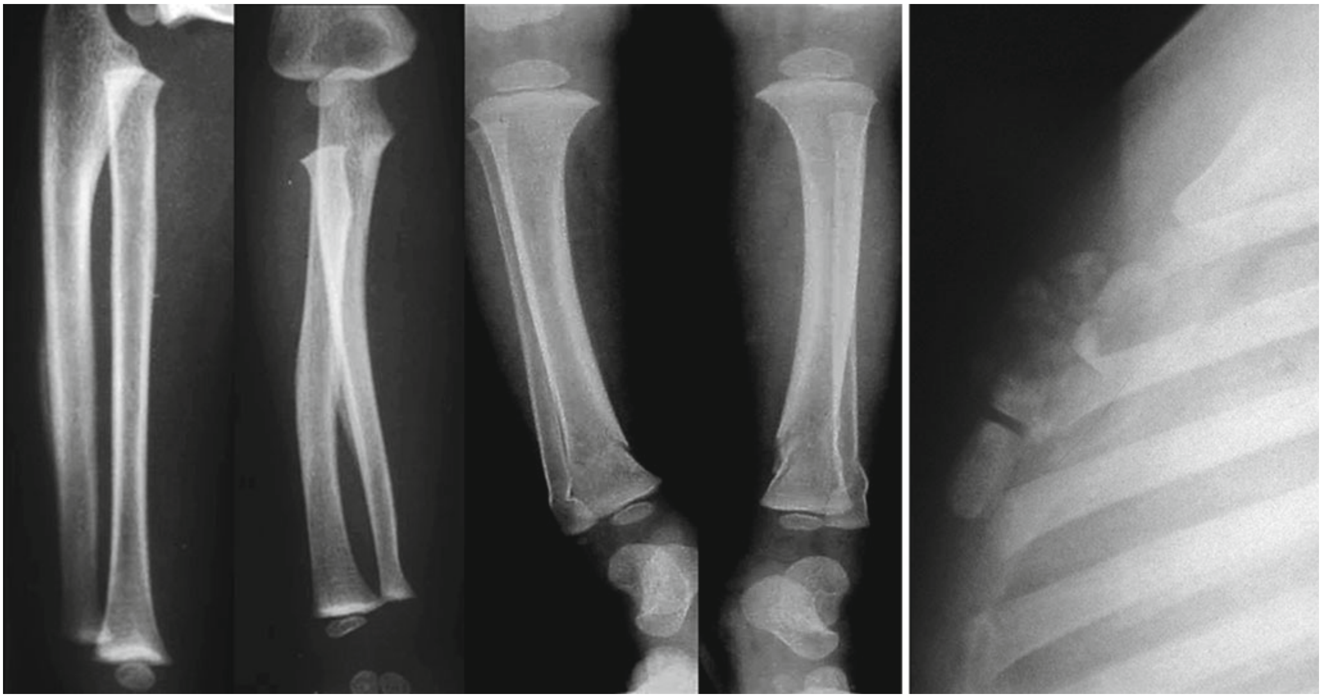

Fig. 9.52 Radiographic findings in two children victims of physical abuse. At *left*, radiographs of the forearms and of the legs display focal areas of periosteal reaction in the mid-diaphyses of the right ulna and of the left radius, with symmetric and bilateral fractures of the distal diaphyses of the tibiae and fibulae. At *right*, lateral view discloses a destructive lesion of the body of the sternum, with ill-defined borders, bone fragmentation, and anterior displacement of its lower portion, related to osteomyelitis (the child was victim of recurrent burns on the anterior portion of the chest, intentionally caused by lit cigarettes)

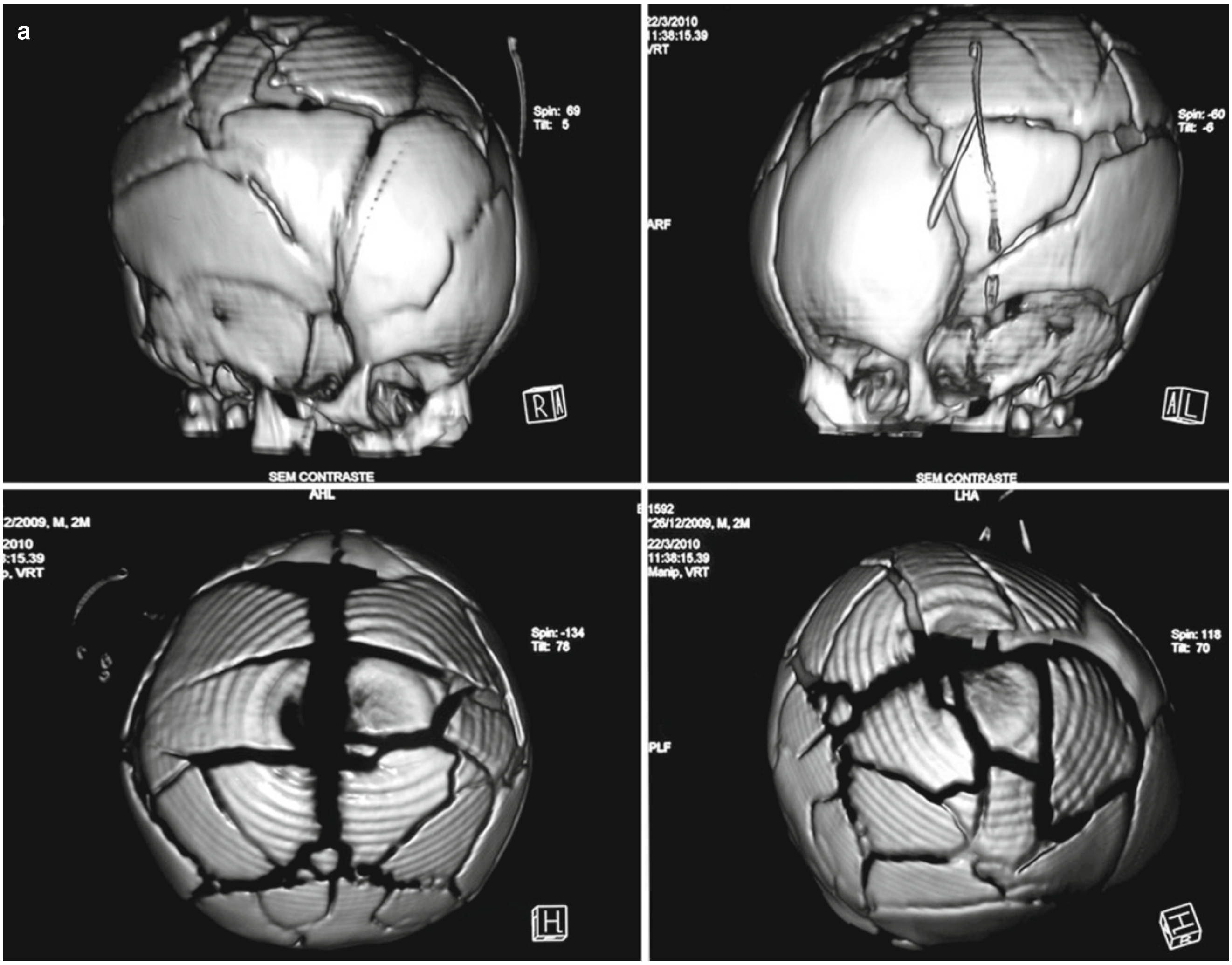

Fig. 9.53 A 2-month-old child admitted to the intensive care unit victim of physical abuse. In (**a**), volume-rendered CT reconstructions demonstrate a complex, multi-fragmented skull fracture that was associated with bilateral subdural collections and brain contusions (not shown). In (**b**), radiographs of the upper limbs of the same child disclose multiple fractures in different stages of healing: spiral diaphyseal fractures of the bones of the left forearm and a transverse fracture of diaphysis of the homolateral humerus (which presents diastasis, angulation, and fragmentation) can be seen, as well as a homolateral supracondylar fracture. There is a complete fracture with gross displacement of the distal portion of the right humerus, as well as thick periosteal reaction in the diaphysis. The distal portion of the right forearm is seen in further detail in (**c**): this image reveals subtle corner fractures in the radius and in the ulna, more evident in the former, in which there is also an incomplete metaphyseal fracture associated with mild bowing (Courtesy of Dr. Marcelo Ricardo Canuto Natal, Hospital de Base do Distrito Federal and Pasteur Medicina Diagnostica – Diagnósticos da America S.A., Brasilia, Brazil)

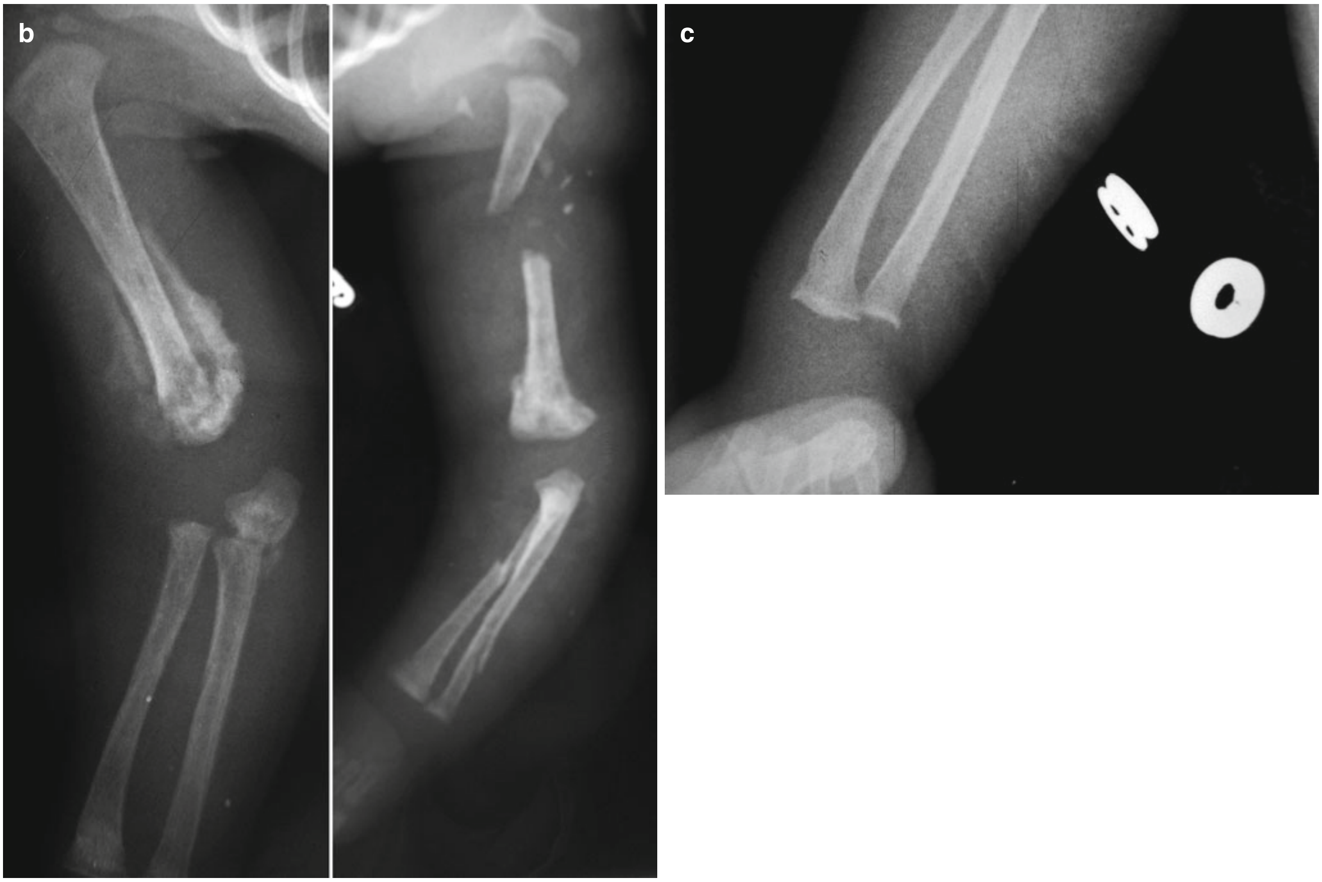

Fig. 9.53 (continued)

Key Points

- Physeal fractures are particularly important because of their potential to cause functional limitation (if the joint surface is affected) and impaired bone growth (damage to the growth cartilage). Salter-Harris classification system divides these fractures into five groups; the prognosis is worst for types III, IV, and V.
- Non-physeal fractures typical of the pediatric population are more common in the forearm, including buckle fractures, greenstick lesions, and plastic deformation. Greenstick fractures deserve special attention because of increased risk of refractures.
- Elbow fractures are the most relevant joint fractures of the upper extremity in children, including supracondylar fractures, fractures of the lateral condyle of the humerus, avulsion fractures of the ossification centers, Monteggia's fracture, and Galeazzi fracture.
- In children, joint fractures are found less often in the lower extremities if compared to the upper extremities, affecting the knees and the ankles in most cases.
- The imaging appearance of the traumatic lesions of the soft tissues in children is essentially the same of those seen in adults. Full-thickness tears of tendons and ligaments are less common in children than in adult patients.
- The radiographic skeletal survey is crucial in the investigation of children with suspected physical abuse. The most important findings include multiple fractures (especially when symmetric and/or in different stages of healing), classic metaphyseal lesions, fractures in atypical sites, and multiple areas of periosteal reaction.

Recommended Reading

Carr KE (2003) Musculoskeletal injuries in young athletes. Clin Fam Pract 5(2):385–415

Carson S, Woolridge DP, Colletti J, Kilgore K (2006) Pediatric upper extremity injuries. Pediatr Clin North Am 53(1):41–67

Chambers HG (2003) Ankle and foot disorders in skeletally immature athletes. Orthop Clin North Am 34(3):445–459

Davis KW (2010) Imaging pediatric sports injuries: lower extremity. Radiol Clin North Am 48(6):1213–1235

Ecklund K, Jaramillo D (2001) Imaging of growth disturbance in children. Radiol Clin North Am 39(4):823–841

Emery KH (2006) Imaging of sports injuries of the upper extremity in children. Clin Sports Med 25(3):543–568

Emery KH (2009) MR imaging in congenital and acquired disorders of the pediatric upper extremity. Magn Reson Imaging Clin N Am 17(3):549–570

Laine JC, Kaiser SP, Diab M (2010) High-risk pediatric orthopedic pitfalls. Emerg Med Clin North Am 28(1):85–102

Lane WG (2003) Diagnosis and management of physical abuse in children. Clin Fam Pract 5(2):493–514

Mulligan ME (2000) Ankle and foot trauma. Semin Musculoskelet Radiol 4(2):241–253

Nimkin K, Kleinman PK (2001) Imaging of child abuse. Radiol Clin North Am 39(4):843–864

Sanchez TR, Jadhav SP, Swischuk LE (2009) MR imaging of pediatric trauma. Magn Reson Imaging Clin N Am 17(3):439–450

Sofka CM, Potter HG (2002) Imaging of elbow injuries in the child and adult athlete. Radiol Clin North Am 40(2):251–265

van Rijn RR, Sieswerda-Hoogendoorn T (2012) Educational paper: imaging child abuse: the bare bones. Eur J Pediatr 171(2): 215–224

White N, Sty J (2002) Radiological evaluation and classification of pediatric fractures. Clin Ped Emerg Med 3(2):94–105